

## Development of Continuum Damage in the Creep Rupture of Notched Bars

D. R. Hayhurst, P. R. Dimmer and C. J. Morrison

*Phil. Trans. R. Soc. Lond. A* 1984 **311**, 103-129  
doi: 10.1098/rsta.1984.0021

### Email alerting service

Receive free email alerts when new articles cite this article - sign up in the box at the top right-hand corner of the article or click [here](#)

To subscribe to *Phil. Trans. R. Soc. Lond. A* go to: <http://rsta.royalsocietypublishing.org/subscriptions>

# DEVELOPMENT OF CONTINUUM DAMAGE IN THE CREEP RUPTURE OF NOTCHED BARS

BY D. R. HAYHURST, P. R. DIMMER AND C. J. MORRISON

*University of Leicester, Engineering Department, Leicester LE1 7RH, U.K.*

*(Communicated by B. A. Bilby, F.R.S. – Received 27 June 1983)*

[Plates 1–4]

## CONTENTS

	PAGE
1. INTRODUCTION	104
2. CONSTITUTIVE EQUATIONS AND DAMAGE LAWS	107
( <i>a</i> ) Uni-axial relations	107
( <i>b</i> ) Multi-axial relations	108
( <i>c</i> ) Normalization	109
( <i>d</i> ) Material data	109
3. CREEP RUPTURE AND THE FINITE ELEMENT DISPLACEMENT METHOD	110
4. RESULTS	112
( <i>a</i> ) Experimental	112
( <i>b</i> ) Theoretical	113
5. DISCUSSION	120
6. CONCLUSIONS	124
APPENDIX	125
REFERENCES	128

The creep rupture of circumferentially notched, circular tension bars which are subjected to constant load for long periods at constant temperature is studied both experimentally and by using a time-iterative numerical procedure which describes the formation and growth of creep damage as a field quantity. The procedure models the development of failed or cracked regions of material due to the growth and linkage of grain boundary defects. Close agreement is shown between experimental and theoretical values of the representative rupture stress, of the zones of creep damage and of the development of cracks for circular (Bridgman, *Studies in large plastic flow and fracture*, New York: McGraw-Hill (1952)) and British Standard notched specimens (B.S. no. 3500 (1969)). The minimum section of the circular notch is shown to be subjected to relatively uniform states of multi-axial stress and damage while the B.S. notch is shown to be subjected to non-uniform stress and damage fields in which single cracks grow through relatively undamaged material. The latter situation is shown to be

analogous to the growth of a discrete crack in a lightly damaged continuum. The continuum damage mechanics theory presented here is shown to be capable of accurately predicting these extreme types of behaviour.

## 1. INTRODUCTION

In the design of engineering structures for operation at high temperatures in the creep range consideration must be given to the possibility of failure arising from creep rupture. In the case of structures that are either uniformly stressed or that contain moderately low stress concentrators, design techniques have been developed which take account of two aspects of material behaviour. These are (i) the increased strain rates that occur during tertiary creep, and (ii) the multi-axial stress rupture criterion satisfied by the material. These new developments are either being included in or have been taken account of in design codes (Hayhurst 1979) for structures which contain moderate stress concentrators. In the case of structures that contain defects or initial cracks the current design codes (B.S. 5500 1982 and A.S.M.E. code case N47 1977) make no recommendations. In these circumstances failure usually takes place by the propagation of a single crack, and the design task reduces to the prediction of the time required for the crack to grow to an unstable length. The methods currently used to predict the lifetimes of cracked components are based on extensions of fracture mechanics to high temperature design conditions, and assume that a single crack grows in mode I in its original plane. More reliable procedures for the design of cracked components, which reflect the governing physical processes, must ultimately require the development of constitutive equations that describe the deformation and rupture behaviour under crack tip conditions and the establishment of numerical methods for the solution of boundary value problems in which cracks propagate due to creep.

The rupture behaviour of structures with moderately low stress concentration factors has been studied by Hayhurst (1973) and by Hayhurst *et al.* (1975) using the concept of continuum damage mechanics and numerical methods for structural analysis. These studies used simple constitutive equations to model the development of tertiary creep strains and a broad class of multi-axial rupture behaviour. Experimental studies, done as part of the same investigations, showed that the main body of the structure undergoes continuum damage, which was observed in the form of grain boundary cavities or fissures; the damage tended to be uniformly distributed throughout uniformly stressed regions, and, in the same way, fields of damage were found to coincide with fields of stress and strain (Hayhurst & Leckie 1973), hence the term continuum damage. Hayhurst *et al.* (1981) have made similar observations in the case of crack components where damage has been observed ahead of the growing crack. Before attempting to apply similar numerical techniques for structural analysis to structures where high stress gradients and complex states of stress are encountered, such as in cracked members, it is first appropriate to use them in situations where moderately high stress concentrations are found, such as in axisymmetric notched tension bars.

Two such structures are the subject of the study reported here; they have been used previously, both experimentally and theoretically with approximate methods of analysis. They are the circular notch due to Bridgman (1952) and the British Standard notch (B.S. no. 3500 1969). Their geometry is defined in figure 1, for a single quadrant, by using cylindrical polar coordinates  $(r, \theta, z)$ . These notches have been studied under stationary-state creep conditions by Hayhurst & Henderson (1977) and under creep damage and rupture conditions by Hayhurst

*et al.* (1978) using an approximate solution for the behaviour at the minimum section ( $z = 0$ ); in addition, the structures typify two extreme conditions: in the circular notch a significant region of the body is subjected to a uniform state of complex stress and in the B.S. notch, complex stress states and high stress gradients are found close to the notch. In the former situation it has been shown by Hayhurst & Henderson (1977) that the spatial variations in the stationary-state stress are small in the vicinity of the minimum section of the notch; this observation has been used by Morrison (1976), Loveday & Dyson (1979) and by Needham & Gladman (1980) to enable material elements to be subjected to relatively uniform states of multi-axial stress. The last condition is of interest since it is characteristic of the conditions found at sharp cracks, but is

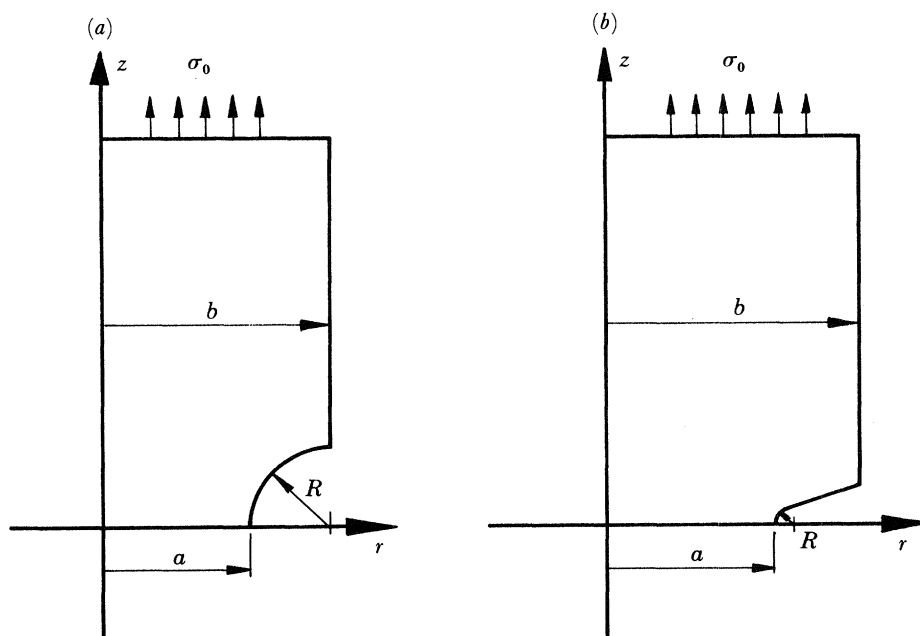


FIGURE 1. Bar geometries for (a) circular notch bar ( $R/a = 0.67$ ,  $b/a = 1.67$ ) and (b) British Standard (B.S.) notch bar ( $R/a = 0.055$ ,  $b/a = 1.41$ ).

simpler to study since it avoids the singular fields found in crack tip problems. The majority of previous theoretical studies have been concerned with the prediction of lifetimes of notched specimens for different materials and geometries. In discussions of such results it is convenient to introduce the normalized representative rupture stress. The performance of a notched specimen may be expressed in terms of the average stress which acts on the minimum section of the notch  $\sigma_n = P/\pi a^2$ , where  $a$  is the radius of the minimum section of the notch and  $P$  is the applied tension load, compared with the stress,  $\sigma_r$ , in a parallel sided uni-axial creep specimen which has the same lifetime as the notched bar. The normalized representative rupture stress  $\Sigma_r$  is defined by  $\sigma_r/\sigma_n$ . A specimen which requires a lower uni-axial stress  $\sigma_r$ , than the average stress  $\sigma_n$  is said to be notch strengthening ( $\Sigma_r < 1$ ) and, conversely a specimen which requires a higher uni-axial stress  $\sigma_r$ , than the average stress  $\sigma_n$  is said to be notch weakening ( $\Sigma_r > 1$ ). Both notch strengthening and weakening can be observed in tests done either on the same material, by changing the specimen geometry, or on the same specimen, by selecting appropriate materials. In an earlier study Leckie & Hayhurst (1974) have shown how notch strengthening and weakening in circular notched specimens can be accurately predicted by consideration of the stress

redistribution effects due to tertiary creep and of the multi-axial stress rupture criterion of the material; the solutions obtained were approximate since the effects of elasticity were neglected and the solution method used the stationary-state stress field as a starting point. An aluminium alloy and copper were selected to represent extreme classes of multi-axial stress rupture behaviour. The aluminium alloy obeys a maximum effective stress,  $\sigma_e (= (\frac{3}{2}S_{ij}S_{ij})^{\frac{1}{2}})$ , rupture criterion, where  $S_{ij} = \sigma_{ij} - \frac{1}{3}\sigma_{kk}\delta_{ij}$ , and the copper is thought to obey a predominantly maximum principal tension stress,  $\sigma_1$ , rupture criterion. Both the theoretical and experimental studies showed that the aluminium alloy and copper specimens exhibited notch strengthening and notch weakening respectively. The study of circular and B.S. notched bars done by Hayhurst *et al.* (1978) using the stationary-state solutions due to Hayhurst & Henderson (1977), made the assumption that the deformation field at the minimum section ( $z = 0$ ) is kinematically determinate. Very good predictions were obtained of the experimental representative rupture stresses, despite the elastic effects being neglected and the theoretical solution being formulated for a thin disc of material, located at the minimum section of the notch. Optical microscopy done on all notched specimens close to failure showed that the behaviour was confined to the minimum sections of the notched bars. The good predictions of notch behaviour may be fortuitous since the field of rupture or damage could deviate from the minimum section for other classes of material behaviour, in addition the effects of elasticity in other crack situations could well be important.

In the work reported here these deficiencies will be overcome, by using constitutive equations capable of describing tertiary creep and the multi-axial behaviour of the material in conjunction with a newly developed finite element system, in a study of the behaviour of circular and B.S. notched specimens for materials that satisfy different multi-axial stress rupture criteria. The constitutive equations used are based on the single state damage variable theory developed by Hayhurst *et al.* (1978). The equations essentially model the physical mechanisms that are known to take place at low stress levels and at high temperatures, typical of those found in engineering components which operate for  $10^5$  h, namely the nucleation, growth and linkage of grain boundary defects. The increased strain rates that take place due to these mechanisms may be described by a single state damage variable theory for situations that are close to proportional loading (Leckie & Hayhurst 1977). The representation is consistent with the operation of a single physical mechanism. The domains of stress and temperature over which the mechanism operates may be determined from the mechanism-maps due to Ashby (1972). The numerical solution procedure is a development of that due to Hayhurst (1973) and of the finite element system developed by Hayhurst *et al.* (1975). The method takes the elastic solution, for a steadily loaded structure, as the starting point and allows creep strain and creep damage to accumulate. When the value of creep damage locally achieves a set value then the region is deemed to have failed; the size of the failed region increases with the further elapse of time until it has spread across a critical region of the structure, when total collapse occurs. The method overcomes the difficulties associated with previous work and, in addition, has the advantage that it can model the behaviour of bodies that contain sharp cracks.

The purpose of the paper is to present full continuum damage solutions for the circular and B.S. notches under conditions of isothermal, steady load creep, to validate the numerical procedures for a range of material behaviour by comparing theoretical results with those of experiments, and to gain a better understanding of the mechanisms by which cracks grow by creep.

The study has been done for three materials. As in previous investigations (Hayhurst *et al.* 1975) an aluminium alloy and copper have been selected as being representative of extreme



classes of multi-axial behaviour; 316 stainless steel has been selected because of its technological significance as a candidate material for the fast breeder nuclear reactor.

Numerical and experimental results will be presented for circular and B.S. notches; theoretical representative rupture stresses will be compared with experimental values; the predicted creep damage fields will be compared with those obtained by using optical metallography. The use of the circular notch specimen as a materials test will be re-examined in the light of the numerical solutions presented here. The characteristics of the stress fields ahead of propagating regions of damage will be studied and a discussion will be presented of their relevance to structures that contain sharp cracks.

## 2. CONSTITUTIVE EQUATIONS AND DAMAGE LAWS

### (a) *Uni-axial relations*

Constitutive equations have been proposed by Kachanov (1958), Hayhurst (1973) and Leckie & Hayhurst (1974) to describe both secondary and tertiary creep. The different methods are essentially the same and involve the usage of a single state damage variable theory in which the creep strain rate  $\dot{\nu}$  is given by

$$\dot{\nu} = f(\sigma, \omega), \quad (1)$$

where  $\omega$  is a state damage variable which is, in some sense, a measure of the cracking or damage in the material. The rate of change of damage is given in terms of the nominal stress  $\sigma$  and the current value of  $\omega$  by

$$\dot{\omega} = g(\sigma, \omega). \quad (2)$$

By appropriate selection of the functions  $f$  and  $g$  it is possible to represent the tertiary portion of the creep curve and to produce stress–lifetime relations consistent with experimental observations. Kachanov's theory, for low values of stress, has been shown by Odqvist & Hult (1961) to be equivalent to the cumulative damage theory due to Robinson (1952).

The physical character of the material damage will not be discussed here since it has been reviewed in detail elsewhere (Hayhurst *et al.* 1975; Hayhurst *et al.* 1978; Leckie & Hayhurst 1977). The physical process that controls the growth of damage, in particular the process of nucleation (Hayhurst *et al.* 1983), is insufficiently well understood to give much insight into the possible form of a general theory. But the accepted quantitative physical theories, in particular those due to Greenwood (1973) and Dyson & McLean (1977), have been shown by Leckie & Hayhurst (1977) to be adequately represented by a single state damage variable theory.

Simple forms of the strain rate (1) and damage (2) equations which can be used to describe the uni-axial behaviour of low stress rupture are given by

$$\dot{\epsilon} = G[\sigma/(1-\omega)]^n, \quad \dot{\omega} = C\sigma^\chi/(1-\omega)^\phi, \quad (3a, b)$$

where  $G$ ,  $C$ ,  $n$ ,  $\chi$  and  $\phi$  are material constants. When the material is undamaged  $\omega = 0$  and (3a) reduces to Norton's law. Rupture is defined by  $\omega = 1$ , when the strain rates are infinitely large. These conditions may be used in the integration of (3b) to obtain the following relation between the rupture time,  $t_r$  and the applied stress

$$t_r = [1/C(1+\phi)]\sigma^{-\chi}. \quad (4)$$

The values of the constants  $C$  and  $\chi$  are obtained from the rupture curve,  $\phi$  is selected to achieve the best description of tertiary strains, while  $G$  and  $n$  may be obtained from secondary creep strain rate data.

(b) *Multi-axial relations*

For secondary creep, multi-axial experimental results by Johnson *et al.* (1962) have confirmed that the creep strain rates are dependent upon the effective stress  $\sigma_e$ , and that the strain rates are normal to the surfaces of constant energy dissipation. This result may be expressed for incompressible creep, following Odqvist (1974), in the form

$$\dot{v}_{ij} = G\{\partial[\Psi^{n+1}(\sigma_{kl})/(n+1)]/\partial\sigma_{ij}\}f(t), \quad (5)$$

where  $f(t)$  is a function of time (usually of the form  $t^m$ ),  $G$ ,  $n$  and  $m$  are material constants and  $\Psi(\sigma_{kl})$  is a homogeneous potential function of degree 1 in stress. Leckie & Hayhurst (1974) have investigated experimental results obtained from tension-torsion tests on copper and on an aluminium alloy and have shown that for both cases the ratio of the axial and shear strain rate components remains approximately constant and equal to the value observed for secondary creep. Consequently the creep strain rates during the primary, secondary and tertiary regions may be represented by an equation of the form

$$\dot{v}_{ij} = G\{\partial[\Psi^{n+1}(\sigma_{kl})/(n+1)]/\partial\sigma_{ij}\}f(t)/(1-\omega)^n, \quad (6)$$

where  $\omega$  represents a scalar measure of creep damage.

The results of several multi-axial stress creep-rupture tests have been collected together by Hayhurst (1972) and used to define classes of isochronous rupture surfaces in bi-axial principal stress space. Two extreme material classifications were made. In the first category the rupture time is governed by a maximum principal tension stress criterion; the behaviour of copper and nimonic alloys is approximately described by this criterion. In the second classification the rupture time is dependent upon the maximum effective stress. For the maximum principle tension stress criterion the rate of increase of  $\omega$  is expressed in terms of the principal stresses  $\sigma_I$ ,  $\sigma_{II}$ ,  $\sigma_{III}$  ( $\sigma_I > \sigma_{II} > \sigma_{III}$ ) by

$$\dot{\omega} = C\sigma^x/(1-\omega)^\phi, \quad (7)$$

and for the maximum effective stress criterion the corresponding relation is

$$\dot{\omega} = C\sigma_e^x/(1-\omega)^\phi. \quad (8)$$

A number of materials, including austenitic stainless steels, obey mixed criteria, in these situations the rate of increase of  $\omega$  may be expressed by

$$\dot{\omega} = C[\alpha\sigma_I + (1-\alpha)\sigma_e]^x/(1-\omega)^\phi, \quad (9)$$

where  $\alpha$  is a factor to be determined from two sets of creep tests, each carried out under a different multi-axial stress state. The most convenient stress state to use in an experimental sense is the uni-axial and probably the second most convenient is the pure shear ( $\sigma_I = -\sigma_{II}$ ,  $\sigma_{III} = 0$ ), which can be carried out on a thin tube subjected to an axial torque. The latter test, while being convenient and capable of differentiating between theories having slightly different  $\alpha$  values, can be influenced in an adverse way by the effects of large deformations, as described by Hayhurst & Storåkers (1976). An alternative to the pure shear test is the circular notch specimen, figure 1, which has been used by Dyson & Loveday (1981) and by Hayhurst *et al.* (1978) as a materials test. However, one deficiency of this approach is that approximate stress fields have been used so far. The solution provided in this paper will be used as a means of establishing the  $\alpha$  values for copper and for stainless steel. The value of  $\alpha$  for aluminium is more firmly established and it has been shown (Hayhurst 1972; Hayhurst & Storåkers 1976) that  $\alpha = 0$ .

The material model used here is essentially for low stress behaviour and it is not intended to model widespread time-independent plasticity either on initial loading of the structure or at the end of the lifetime when an instantaneous plastic collapse mechanism may operate. In the solution of the boundary value problem, localized plasticity may be modelled reasonably well since the  $n$ -power stress behaviour of the constitutive equations is the same for creep and for plasticity (Penny & Hayhurst 1969).

(c) *Normalization*

To enable the time scales of (6) and (9) to be normalized in the same way, (9) is rewritten as

$$\dot{\omega} = M[\alpha\sigma_1 + (1-\alpha)\sigma_e]^\chi f(t) / [(1+\phi)(1-\omega)^\phi], \quad (10)$$

where  $f(t)$  ( $= t^m$ ) is the time function in (6) and  $M$  is a constant. This step involves a slight redefinition of the time scale in (9), which has been justified by Hayhurst (1970). It is convenient now to introduce the normalized parameters

$$\begin{aligned} \Sigma_{ij} &= \sigma_{ij}/\sigma_0, & V_{ij} &= v_{ij}/e_0, \\ \xi_{ij} &= e_{ij}/e_0, & \lambda_{ij} &= \epsilon_{ij}/e_0, \end{aligned}$$

where  $\sigma_0$  is a constant stress which has been selected as the uniform stress applied to the parallel region of the notched bar (cf. figure 1), where  $e_0$  is the uni-axial elastic strain given by  $\sigma_0/E$ , and  $E$  is Young's modulus. Equation (6) can then be redefined and rewritten as

$$\dot{V}_{ij} = GE\sigma_0^{(n-1)} t^m \{ \partial[\Psi^{n+1}(\Sigma_{kl})/(n+1)] / \partial \Sigma_{ij} \} / (1-\omega)^n. \quad (11)$$

The material constants can be eliminated from this expression by introduction of the normalized time

$$\tau = \int_0^t GE\sigma_0^{(n-1)} t^m dt,$$

discussed by Hayhurst (1973) and obtained by dividing the uni-axial creep strain, calculated from (5), by the elastic strain at the stress  $\sigma_0$ . Equation (11) when expressed in terms of the normalized time becomes

$$\dot{V}_{ij} = dV_{ij}/d\tau = \{ \partial[\Psi^{n+1}(\Sigma_{kl})/(n+1)] / \partial \Sigma_{ij} \} / (1-\omega)^n. \quad (12)$$

In the same way, the normalized rate of change of  $\omega$ , given by (10), can be rewritten as

$$\dot{\omega} = d\omega/d\tau = [\alpha\Sigma_1 + (1-\alpha)\Sigma_e]^\chi / V_u (1+\phi)(1-\omega)^\phi, \quad (13)$$

where  $\Sigma_1$  is the normalized maximum principal stress and  $V_u$  is a constant, equal to the normalized creep strain computed from the uni-axial form of (5) after the rupture life at the stress  $\sigma_0$  and is given by

$$V_u = (GE/M)\sigma_0^{(n-\chi-1)}. \quad (14)$$

(d) *Material data*

Of the three materials used the aluminium alloy, B.S. 1472 tested at  $210 \pm \frac{1}{2}^\circ\text{C}$ , and the commercially pure copper, tested at  $250 \pm \frac{1}{2}^\circ\text{C}$ , have been used in experimental studies carried out on thin plates containing circular holes by Hayhurst *et al.* (1975). The data used in this investigation have been taken from figures 2 and 3 of that paper and are summarized in table 1. The AISI 316 stainless steel material was tested under uni-axial conditions at  $550 \pm 2^\circ\text{C}$  and the experimental creep curves are compared in figure 2 with the computed values; the corresponding data are given in table 1. The procedure used to fit the data involved the digitization of



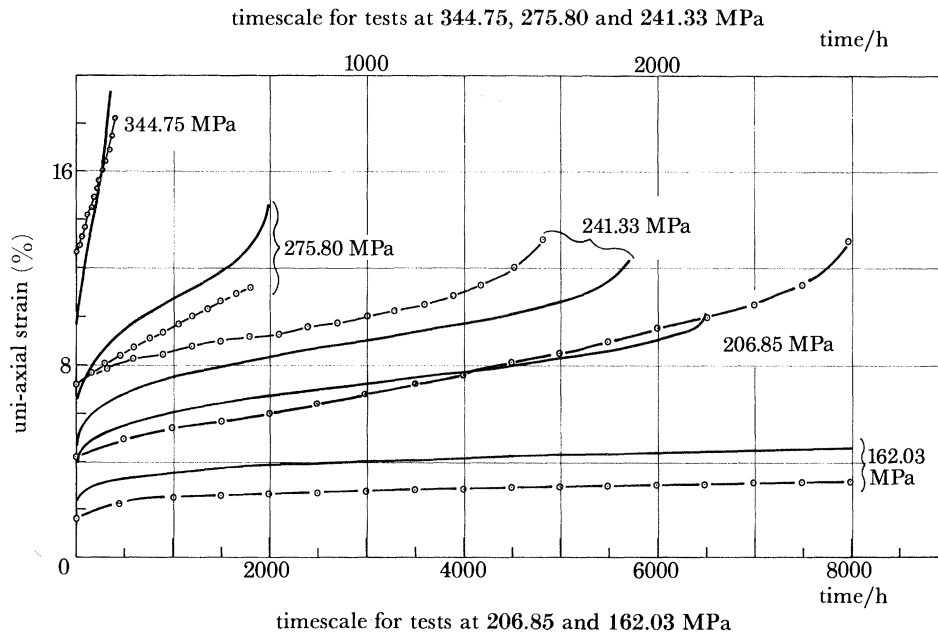


FIGURE 2. Comparison of computed with experimental values of strain for 316 stainless steel (—○—, experiment).

TABLE 1. SUMMARY OF MATERIAL CONSTANTS EXPRESSED IN UNITS OF MEGAPASCALS, PERCENTAGE CREEP STRAIN AND HOURS

parameter	aluminium alloy	copper	316 stainless steel
$E/\text{MPa}$	$60.03 \times 10^3$	$66.24 \times 10^3$	$169.617 \times 10^3$
$\nu$	0.30	0.30	0.300
$n$	6.90	5.00	1.737
$m$	-0.20	-0.43	-0.940
$\chi$	6.48	3.19	0.478
$\phi$	9.50	6.00	1.914
$\alpha$	0	0.70	0.750
$G$	$1.15 \times 10^{-15}$	$3.21 \times 10^{-10}$	$1.383 \times 10^{-5}$
$M$	$1.79 \times 10^{-14}$	$1.89 \times 10^{-7}$	$2.774 \times 10^{-3}$

the creep data, the usage of an optimization procedure that utilized a penalty function to measure the quality of agreement between the computed and experimental data. The procedure, which is semi-automatic, requires little user-control.

The data presented in table 1 will be used together with the multi-axial generalizations, given by (12) and (13), to study the behaviour of both the circular and the B.S. notches. Numerical methods for the solution of the boundary value problems are discussed in the next section.

### 3. CREEP RUPTURE AND THE FINITE ELEMENT DISPLACEMENT METHOD

Single quadrants of the notch bars under investigation are shown in figure 1. Since the bars are symmetrical about the  $z$ -axis, axi-symmetric finite elements can be used to define the body in a single  $(z, r)$ -plane. Only one half of the bar need be considered,  $z \geq 0$ , since the bar is symmetrical about the plane defined by  $z = 0$ . The finite element mesh geometries and the

procedures used to obtain the elastic solutions for the circular and B.S. notches were identical to those used by Hayhurst & Henderson (1977).

The numerical solution of the boundary value problem discussed by Hayhurst *et al.* (1975) utilized a rate formulation. Subsequent experience with this method showed that it is not a particularly well conditioned formulation for the solution of boundary value problems in which the boundary can change with time. The principal deficiency is that if overall equilibrium is to be preserved, to close limits, as the boundary value problem is redefined then prohibitively small integration time-steps are required. Hayhurst & Krzeczowski (1979) have studied the techniques available for the solution of this class of problem and have concluded that a more well-conditioned formulation is obtained when the boundary value problem is solved in terms of the absolute field variables rather than their rate equivalent. In this paper the so called absolute method of solution will be used.

Consider one half of a notched bar to be idealized by using triangular finite elements whose displacements are linear functions of the spatial coordinates. Then for the  $i$ th element the generalized displacement  $\mathbf{u}^i(\mathbf{r}, \mathbf{z})$  are related to a global displacement vector  $\mathbf{U}$  by  $\mathbf{u}^i = \mathbf{N}^i \mathbf{U}$ , where  $\mathbf{N}^i$  is the displacement matrix, which is dependent upon element geometry,  $\mathbf{U}$  and  $\mathbf{u}$  are normalized displacement vectors given by  $\mathbf{U} = U_i/e_0$  and  $\mathbf{u} = u_i/e_0$ . In the same way the elastic strains are given by  $\xi^i = \mathbf{B}^i \mathbf{U}$ , and the isotropic stress-strain relation can be written as

$$\boldsymbol{\Sigma}^i = \mathbf{D} \xi^i = \mathbf{D} \mathbf{B}^i \mathbf{U}, \quad (15)$$

where  $\boldsymbol{\Sigma}$  are the elastic stresses and  $\mathbf{D}$  is a matrix of elastic constants.

The creep strain rates  $\dot{V}_{ij}$  are dependent on the current stress and damage and are expressed by (12) and (13). The total strain  $\lambda$  is composed of an elastic component  $\xi$  and a creep component  $V$ , and is given for the  $i$ th finite element by

$$\lambda^i = \mathbf{B}^i \mathbf{U} = \xi^i + V^i$$

Since  $\boldsymbol{\Sigma}$  is the stress due to the elastic strain  $\xi$  then

$$\mathbf{D} \mathbf{B}^i \mathbf{U} = \boldsymbol{\Sigma}^i + \mathbf{D} V^i. \quad (16)$$

Now consider the boundary value problem for which the nodal load vector  $\mathbf{f}$  is given in terms of the applied load vector  $\mathbf{w}$  by

$$\mathbf{f} = \sum_i \int_{S_i} (\mathbf{N}^i)^T \mathbf{w} dS,$$

where  $S_i$  denotes the element of surface corresponding to the  $i$ th finite element. The principle of virtual work may now be applied to the boundary value problem:

$$\begin{aligned} \mathbf{U}^T \mathbf{f} &= \sum_i \int_{\tilde{V}_i} \lambda^{iT} \boldsymbol{\Sigma}^i d\tilde{V}, \\ &= \sum_i \int_{\tilde{V}_i} (\mathbf{B}^i \mathbf{U})^T (\mathbf{D} \mathbf{B}^i \mathbf{U} - \mathbf{D} V^i) d\tilde{V}, \\ &= \sum_i \mathbf{U}^T \left[ \left\{ \int_{\tilde{V}_i} \mathbf{B}^{iT} \mathbf{D} \mathbf{B}^i d\tilde{V} \right\} \mathbf{U} - \left\{ \int_{\tilde{V}_i} \mathbf{B}^{iT} \mathbf{D} d\tilde{V} \right\} V^i \right], \end{aligned} \quad (17)$$

where  $\tilde{V}_i$  denotes the volume of the  $i$ th element. On substitution of

$$\mathbf{K} = \sum \int \mathbf{B}^{iT} \mathbf{D} \mathbf{B}^i d\tilde{V}$$

for the overall stiffness matrix of the structure, and using

$$A^i = \int B^{iT} D d\bar{V},$$

and  $f^e = \sum_i A^i V^i$  for the nodal creep load vector, (17) becomes

$$f = KU - f^e \quad \text{or} \quad U = K^{-1}(f + f^e). \quad (18)$$

The elastic stresses at  $\tau = 0$  may be derived from (18) with  $f^e = 0$  or

$$f = KU \quad \text{and} \quad U = K^{-1}f. \quad (19)$$

The creep strains and associated damage values at any time may be obtained from the constitutive equations (12) and (13) by using the integration procedures described in the Appendix and the solution to the boundary value problem given by (18) and (16).

In the rupture calculation, failure of an element is assumed to have occurred when  $\omega \geq 0.999$ . When the damage in an element has exceeded this value, the overall stiffness matrix and the boundary conditions are reformulated. Procedures for effecting these changes are now discussed.

When the rupture condition for an element is satisfied, the material is assumed to be no longer capable of transmitting or withstanding force. The overall stiffness matrix is reassembled with the stiffness matrix for the failed element omitted and the new inverse  $K^{-1}$  is formed and stored. The force and displacement conditions for nodes that are associated with several elements that have failed may require inclusion in the boundary conditions. This was achieved by forming the appropriate inverse of the stiffness matrix  $K^{-1}$  and by setting to zero the displacement components of nodes no longer associated with unfailed elements.

It is conceivable that regions of failed elements can form around smaller regions which have not failed. Checks were carried out to test for the presence of these regions, and if such areas existed the elements were assumed to satisfy the rupture conditions and were treated as failed elements.

#### 4. RESULTS

##### (a) *Experimental*

The results of the tests carried out on copper and aluminium alloy bars have been presented elsewhere; graphs in which the average minimum section stress has been plotted against rupture time have been presented by Leckie & Hayhurst (1974) for the circular notch, and values of the representative rupture stress, corrected for notch geometry changes, have been presented by Hayhurst *et al.* (1978). These results are summarized in table 2.

The graph in which the average tensile stress at the minimum section of the notch is plotted against the rupture lifetimes for the circular and B.S. notches in 316 stainless steel is presented in figure 3. The line for the circular notch has been drawn through two experimental points. Test result for higher stresses (over 350 MPa) showed a slight dependence on stress; these results have not been plotted since the theoretical predictions are essentially for low stress behaviour. The corresponding values of the representative rupture stress, corrected for notch geometry changes, in the manner described by Hayhurst *et al.* (1978), are presented in table 2. The circular notch shows notch strengthening for all three materials, the degree of strengthening increasing from copper to stainless steel to the aluminium alloy. The B.S. notch shows a decrease in strengthening from 0.870, for the aluminium alloy to 0.942, for the stainless steel; the copper notch shows a weakening of 1.170.

Optical metallographic studies of all notches have been done and the results will be presented in a later section.

(b) *Theoretical*

The numerical computations were done in double precision on the Science and Engineering Research Council IBM 360/195 computer at the Rutherford and Appleton Laboratory, Chilton. The finite element meshes used for the geometries shown in figure 1 had approximately 500 degrees of freedom. Computer times were of the order of 30 min per run. Solutions were

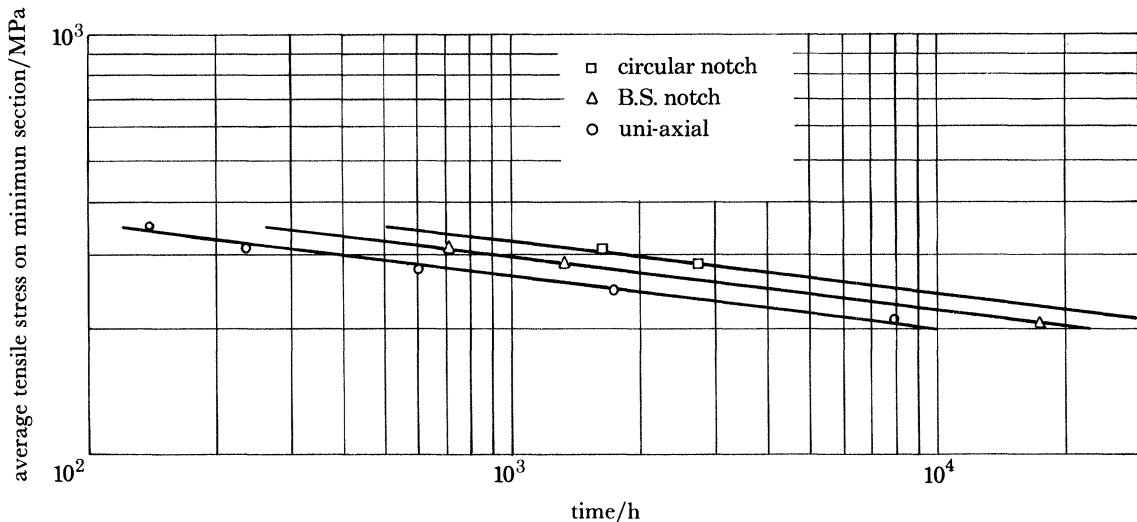


FIGURE 3. 316 stainless steel rupture data for uni-axial, circular and B.S. notch specimens.

TABLE 2. EXPERIMENTAL VALUES OF THE REPRESENTATIVE RUPTURE STRESS

material	normalized representative rupture stress $\Sigma_r$	
	circular notch	British standard notch
copper	0.950	1.170
aluminium alloy	0.740	0.870
316 stainless steel	0.858	0.942

obtained for both notches with data for the aluminium alloy, the copper and the 316 stainless steel with appropriate values of  $\alpha$  for the multi-axial stress rupture criteria. The established value of  $\alpha = 0$  was used in the case of the aluminium alloy (Hayhurst & Storåkers 1976). Values of  $\alpha$  for copper and 316 stainless steel are less well established. For these materials, values of the representative rupture stress,  $\Sigma_r$ , were computed for a range of values of  $\alpha$  and, for each material, the value of  $\alpha$  was selected, which gives the theoretical values of  $\Sigma_r$  consistent with those observed experimentally. The values of  $\sigma_0$  used in the computation of  $V_w$ , from (14), were selected from the lower end of the range of experimental stresses used. However, the computed values of  $\Sigma_r$  were almost independent of the values of  $\sigma_0$ . Theoretical values of the normalized representative rupture stress are compared in figure 4 with experimental values, for both notches in copper. The value  $\alpha = 0.7$  gives close agreement and this value has been used in all calculations reported here. The value  $\alpha = 0.7$  is less than the value of 0.82 obtained by Hayhurst *et al.* (1978), this is most probably due to the approximate character of their method of solution. Had the value of

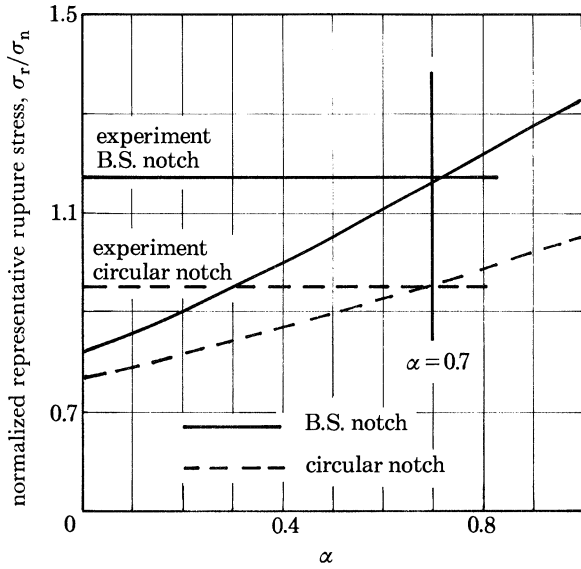


FIGURE 4. Variation of normalized representative rupture stress with  $\alpha$  for copper.

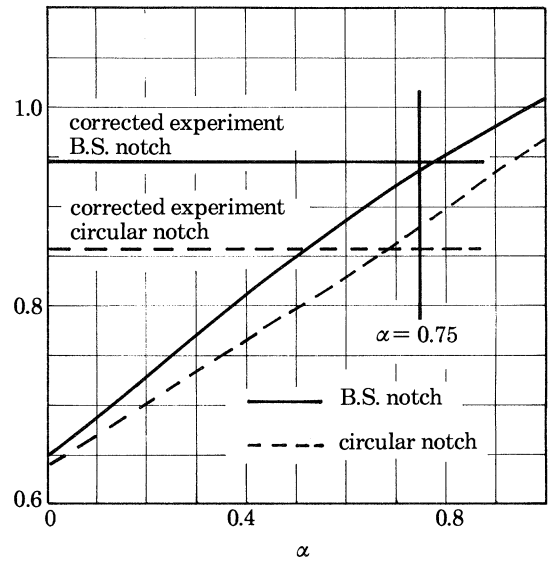


FIGURE 5. Variation of normalized representative rupture stress with  $\alpha$  for 316 stainless steel.

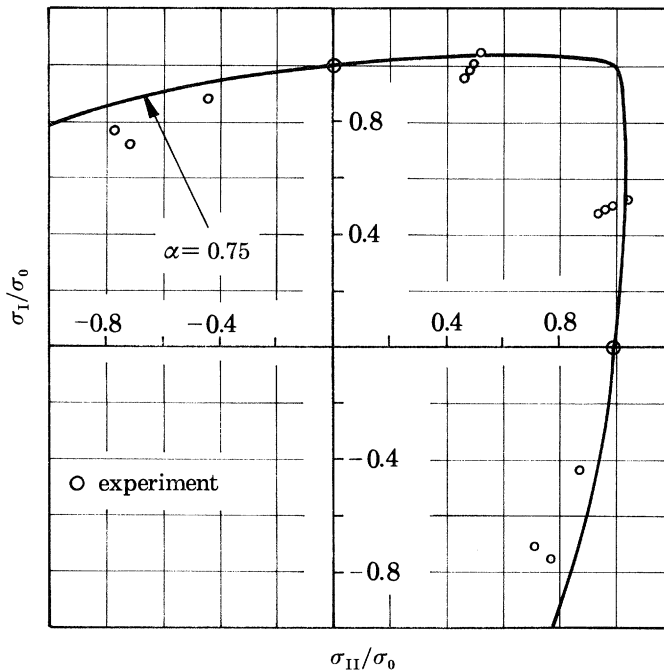


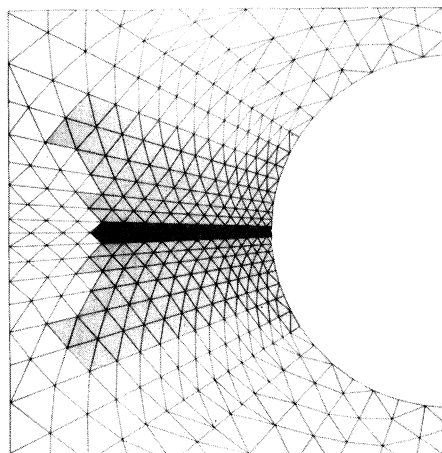
FIGURE 6. Comparison of isochronous rupture loci for  $\alpha = 0.75$  with experimental results obtained for 316 stainless steel at 600 °C by Chubb & Bolton (1980).

$\alpha = 0.7$ , been used in the investigation of the behaviour of the Andrade shear disc (Hayhurst & Storåkers 1976), instead of the value  $\alpha = 1$ , then better agreement may have been obtained between the results of theory and experiment. In addition, the lifetime of a thin copper tube tested by Trampczynski *et al.* (1981) under axial tension and torque had an experimental lifetime of 230 h; theoretical predictions based on (13) with  $\alpha = 1$  and  $\alpha = 0.7$  are 315 h and 290 h





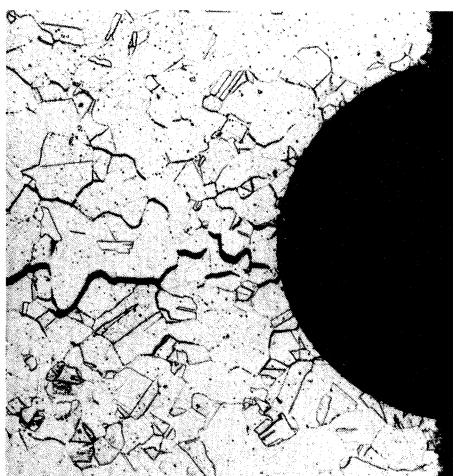
aluminium



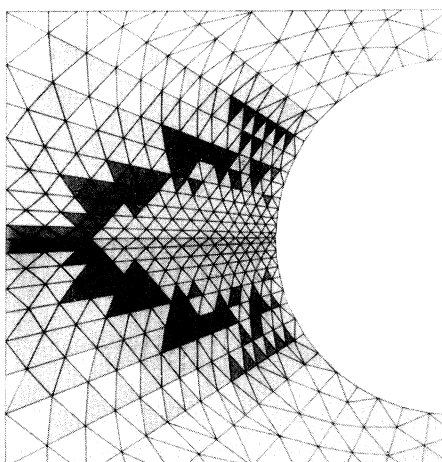
▲  $\omega \geq 0.99$

△  $\omega \geq 0.10$

FIGURE 7. Comparison of a theoretical prediction of the distribution of damage in a circular notched bar with that observed in a micrograph taken from a diametral plane close to failure.



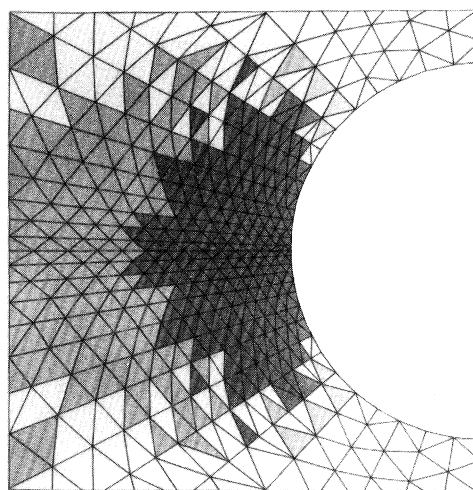
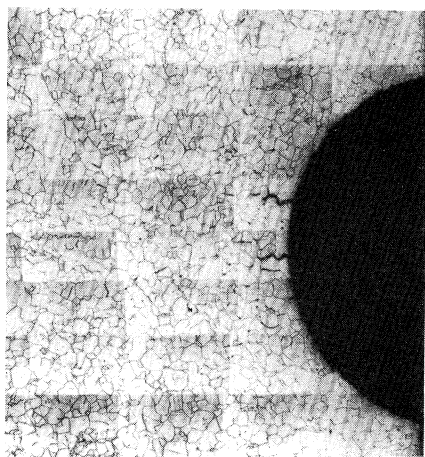
copper




▲  $\omega \geq 0.99$

△  $\omega \geq 0.10$

FIGURE 8. Comparison of a theoretical prediction of the distribution of damage in a circular notched bar with that observed in a micrograph taken from a diametral plane close to failure.



316 stainless steel

  $\omega \geq 0.99$


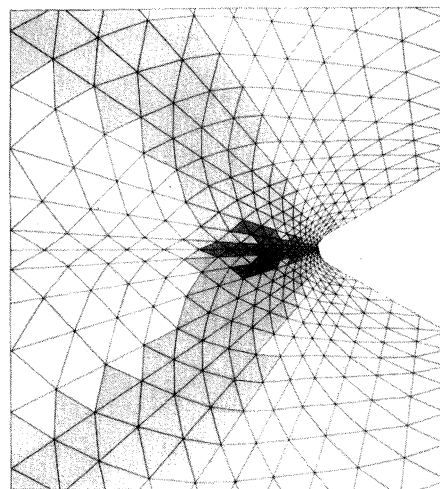

  $\omega \geq 0.10$

FIGURE 9. Comparison of a theoretical prediction of the distribution of damage in a circular notched bar with that observed in a micrograph taken from a diametral plane close to failure.



aluminium

  $\omega \geq 0.99$


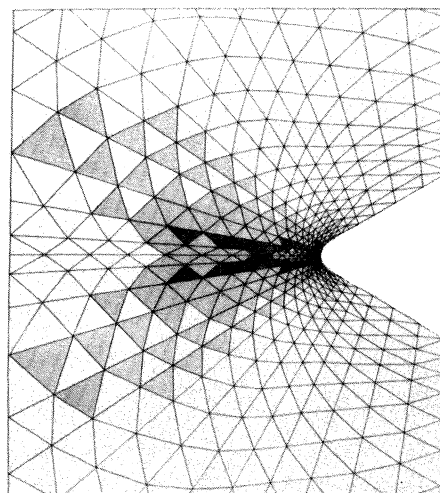
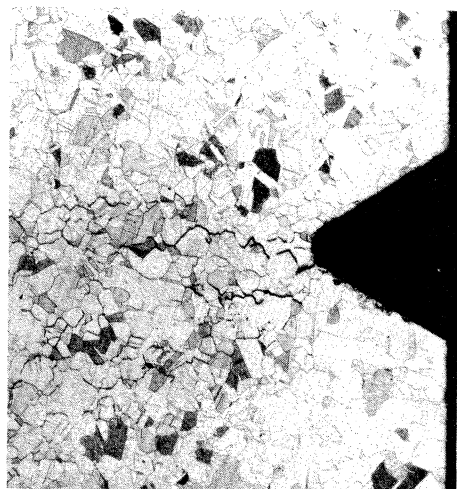

  $\omega \geq 0.10$

FIGURE 13. Comparison of a theoretical prediction of the distribution of damage in a B.S. notched bar with that observed in a micrograph taken from a diametral plane close to failure.



copper

  $\omega \geq 0.99$


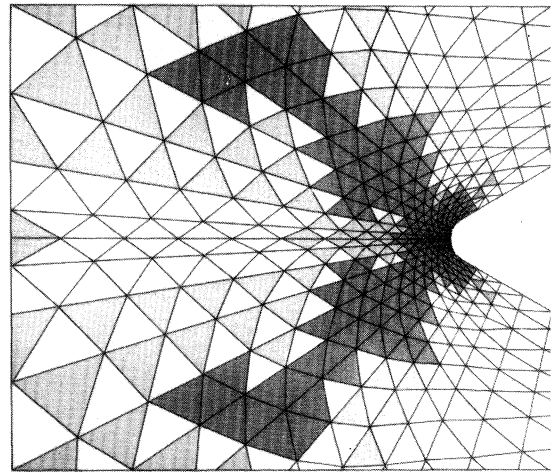
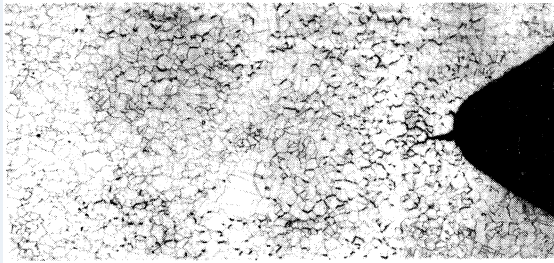
  $\omega \geq 0.10$

FIGURE 14. Comparison of a theoretical prediction of the distribution of damage in a B.S. notched bar with that observed in a micrograph taken from a diametral plane close to failure.





▲  $\omega \geq 0.99$

▲  $\omega \geq 0.10$

316 stainless steel

FIGURE 15. Comparison of a theoretical prediction of the distribution of damage in a B.S. notched bar with that observed in a micrograph taken from a diametral plane close to failure.

respectively. In these tests the ratio of axial to shear stress was arranged to reduce the effects of finite deformations. Both the tension–torsion tube results and the Andrade shear disc results lend support to the value of  $\alpha$ , for copper tested at  $250 \pm \frac{1}{2}^\circ\text{C}$ , being less than unity. Theoretical values of  $\Sigma_r$  for a range of values of  $\alpha$  in 316 stainless steel are compared in figure 5 with experimental values for the circular and B.S. notches. The value  $\alpha = 0.75$  gives close agreement for both notches. The corresponding isochronous surface in bi-axial principal stress space ( $\sigma_{III} = 0$ ) is shown in figure 6 and is compared with experimental results on the same material, tested at  $600^\circ\text{C}$  by Chubb & Bolton (1980), with reasonably good agreement. The value  $\alpha = 0.75$  has been used for stainless steel in all calculations reported here. As one would expect, from the way in which the values of  $\alpha$  have been selected, good agreement has been achieved between the experimental and theoretical values of  $\Sigma_r$  (see table 3).

TABLE 3. COMPARISON OF EXPERIMENTAL WITH THEORETICAL VALUES OF THE REPRESENTATIVE RUPTURE STRESS

material	case	normalized representative rupture stress $\Sigma_r$	
		circular notch	British standard notch
copper	experiment	0.950	1.170
	theory	0.997	1.230
aluminium alloy	experiment	0.740	0.870
	theory	0.771	0.820
316 stainless steel	experiment	0.858	0.942
	theory	0.878	0.936

Computed zones of damage, defined by  $\omega \geq 0.99$  and  $\omega \geq 0.1$ , are shown in figures 7 and 8 (plate 1) and 9 (plate 2), for the circular notch with the aluminium alloy, copper and stainless steel respectively, and are compared with micrographs taken from diametral planes of notches close to failure. This has been achieved by testing bars with two, well separated, identical notches; after failure at one of the notches the second notch is automatically interrupted close to failure and has been used for metallographic examination. It can be seen from figure 7 that for the aluminium alloy, the theory predicts that a single crack propagates through damaged material across the minimum section. In the metallographic section some directionality may be observed in the grain structure and the single crack has propagated at an angle to the  $r$ -axis. In figure 8, for copper, the theoretical damage first forms at the edge of the notch but at a value of  $z > 0$ . The growth of the damage zone does not spread out uniformly from a particular region but occurs in a random fashion at different points over a wide region. Final failure occurs by the ‘filling-in’ of un-failed regions. In figure 9, for 316 stainless steel, a damage region with  $\omega \geq 0.99$  forms at ( $r = a, z = 0$ ) early in the lifetime, it spreads gradually but remains essentially stable for the major part of the life; 316 stainless steel is capable of achieving relatively large creep strains and it would appear that the stable cracking observed is a consequence of this property.

Values of the normalized stress  $\Sigma_{zz}$  are plotted against normalized radial distance  $\bar{r}$  ( $= r/a$ ) for values of the normalized time  $t/t_t$ , where  $t_t$  is the computed real time at failure, in figures 10, 11, and 12 for the three materials with the circular notch geometry. Figure 10 shows the distributions of stress for the aluminium alloy. Although significant stress redistribution has taken place during the first 6.3 % of life it is after 42 % of life that the distribution of stress is similar to the stationary-state distribution due to Hayhurst & Henderson (1977) for  $n = 7$ . Between the normalized times  $t/t_t = 0.063$  and 0.963, when first failure occurs, the stresses remain relatively



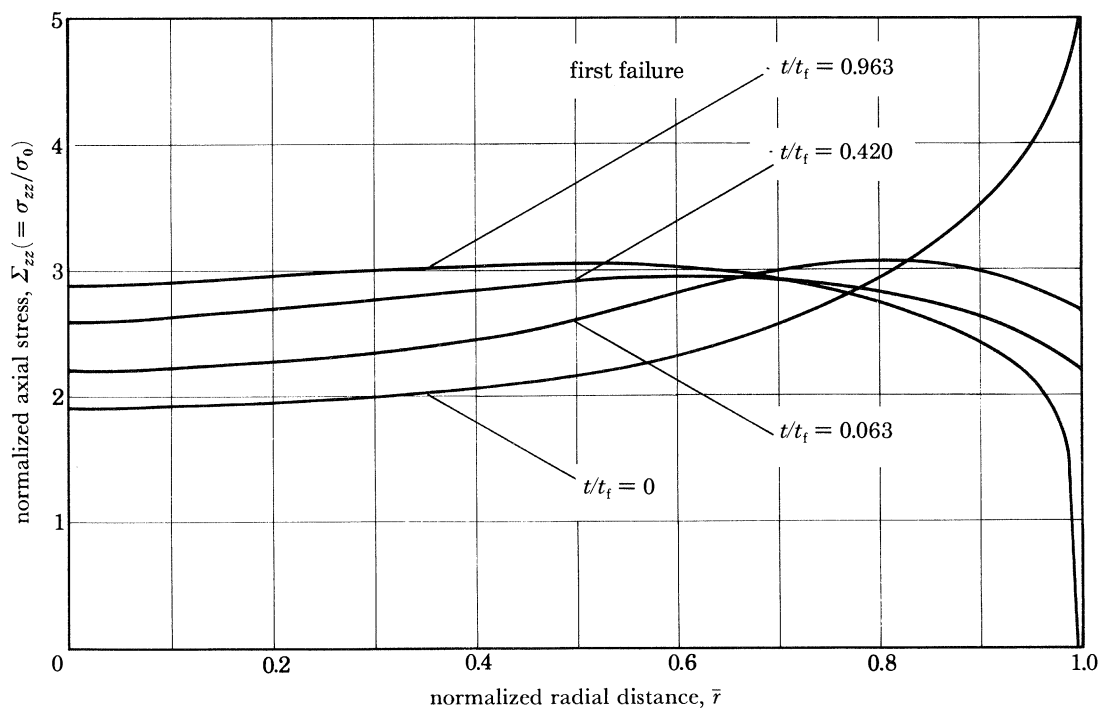


FIGURE 10. The change of normalized axial stress with the normalized time ( $t/t_f$ ) in a circular notch for an aluminium alloy ( $z = 0$ ).

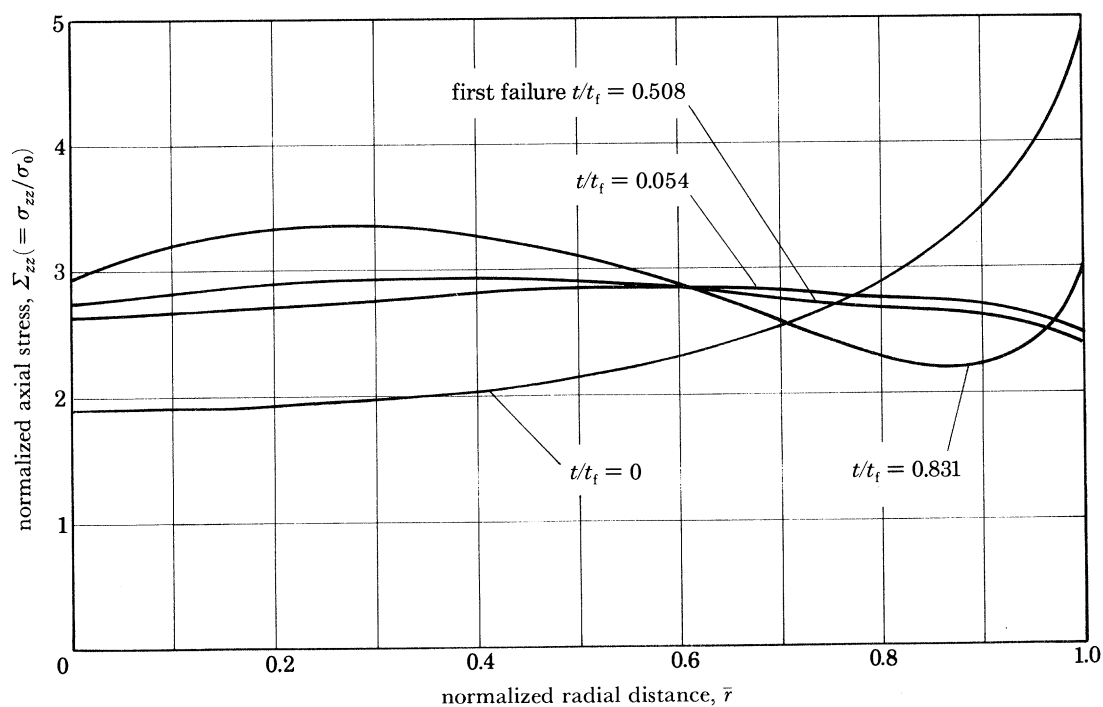


FIGURE 11. The change of normalized axial stress with the normalized time ( $t/t_f$ ) in a circular notch for copper ( $z = 0$ ).

constant, hence justifying the usage of this specimen as a materials test. Figure 11 shows the distributions of stress for copper. Considerable stress redistribution has taken place after 5.4 % of life and the distribution of stress remains essentially constant until the occurrence of the first failure at  $t/t_f = 0.508$ . At the normalized time  $t/t_f = 0.831$  it can be seen that elemental failures removed from the  $r$ -axis have begun to influence the smoothness of the stress distribution. The spatial variation of stress at  $t/t_f = 0.054$  is very similar to the stationary-state variation for  $n = 5$ . Since the stress distributions shown in figure 11 are essentially constant for a significant proportion of the life, the usage of the circular notch specimen may be justified as a materials test for copper. Figure 12 shows the distributions of stress for 316 stainless steel. Considerable stress redistribution has taken place after the first 2.4 % of life when the first failure occurs at the tip

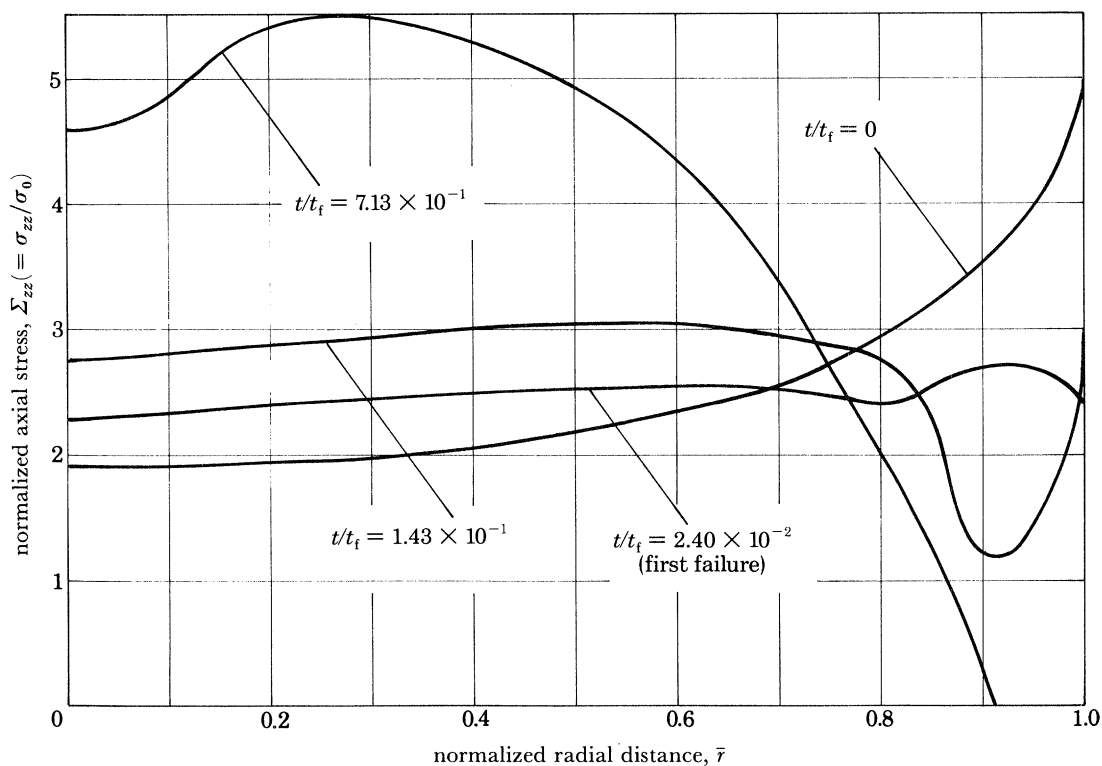


FIGURE 12. The change of normalized axial stress with normalized time ( $t/t_f$ ) in a circular notch for 316 stainless steel ( $z = 0$ ).

of the notch with  $z > 0$ . At 14.3 % of life the stress distribution is non-uniform and at 71.3 % of life has undergone a radical change. The stress distributions shown in figure 12 bear little resemblance to the equivalent extrapolated stationary-state distribution,  $n = 1.74$ , obtained by Hayhurst & Henderson (1977). Clearly the circular notch specimen for this material does not behave, even in an approximate way, like a homogeneously stressed body at the minimum section of the notch, consequently care must be exercised when using this specimen as a materials test for 316 stainless steel.

Computed zones of damage defined by  $\omega \geq 0.99$  and  $\omega \geq 0.1$  are shown in figures 13 and 14 (plate 3) and 15 (plate 4) for the B.S. notch with the aluminium alloy, copper and stainless steel respectively and are compared with micrographs taken from diametral planes of notches close to

failure. The predicted damage zones illustrated in figure 13, for the aluminium alloy, show that damage,  $\omega \geq 0.1$ , has formed on shear planes inclined at approximately  $50^\circ$  to the  $r$ -axis. Despite this a single crack has propagated along the  $r$ -axis. This feature will be examined in more detail in a later section. The micrograph shows that, despite a pronounced directionality of the grain structure, the crack has propagated along the  $r$ -axis; the presence of grain boundary damage in the shear lobes may also be observed. In figure 14, for copper, the predicted damage zones show 'patchy' regions of damage of magnitude  $\omega \geq 0.1$  which spread out in a direction inclined at an angle of approximately  $25^\circ$  to the  $r$ -axis. Two distinct cracks have formed which are inclined at a

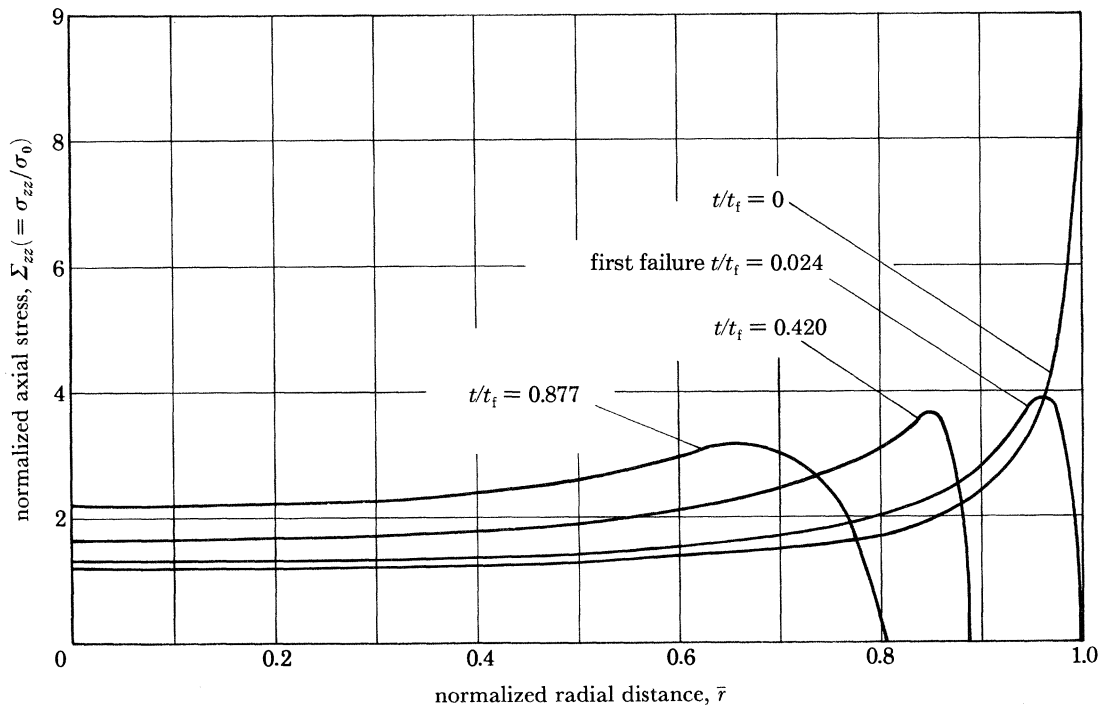


FIGURE 16. The change of normalized axial stress with normalized time ( $t/t_i$ ) in a B.S. notch for an aluminium alloy ( $z = 0$ ).

small angle to the  $r$ -axis. This pattern shows some of the characteristics exhibited by the solution for aluminium, i.e. with  $\alpha = 0$ . The micrograph shows the same predominant features as the theoretical predictions. Different damage characteristics have been predicted for stainless steel, figure 15. In this case the two regions of damage  $\omega \geq 0.99$  and  $\omega \geq 0.10$ , coincide. Regions of intense damage have spread out in directions inclined at approximate angles of  $40^\circ$  to the  $r$ -axis. The micrograph closely reflects the predicted behaviour. The factors that cause the direction of intense damage or cracking to change from the  $r$ -axis, as in the case of the aluminium alloy to directions inclined to the  $r$ -axis, will be studied in a later section.

Smoothed distributions of the normalized stress  $\Sigma_{zz}$  along the  $r$ -axis for values of the normalized time  $t/t_i$  are shown in figures 16, 17 and 18 for the three materials with the B.S. notch. Figure 16 shows the distributions of stress for the aluminium alloy. After 2.4% of the lifetime, when the first crack forms, the stresses have redistributed to values close to the stationary-state ones due to Hayhurst & Henderson (1977), for  $n = 7$ . Thereafter, a crack advances along the  $r$ -axis with a progressively increasing average stress ahead of it; the shape of the distribution being similar to

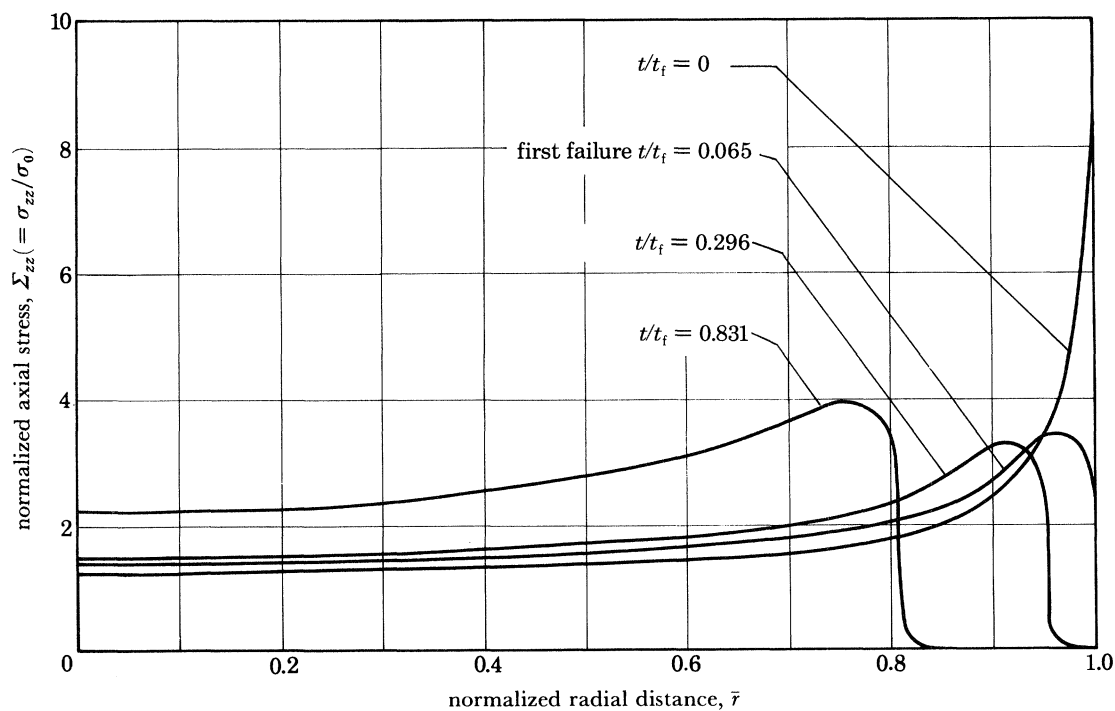


FIGURE 17. The change of normalized axial stress with the normalized time ( $t/t_i$ ) in a B.S. notch for copper ( $z = 0$ ).

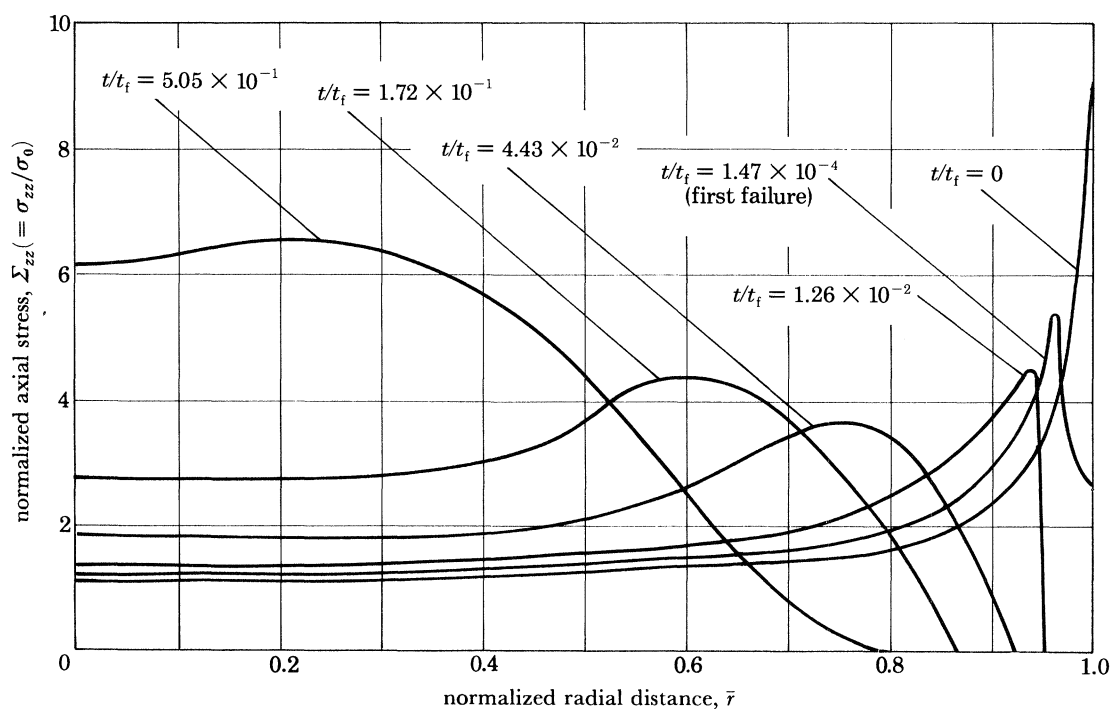


FIGURE 18. The change of normalized axial stress with normalized time ( $t/t_i$ ) in a B.S. notch for 316 stainless steel ( $z = 0$ ).

that for the stationary-state. The spatial distributions of stress for copper shown in figure 17, are similar in style to those for the aluminium alloy. After 6.5 % of life the first crack forms, at this time the stress distribution is different from the equivalent stationary-state solution,  $n = 5$ . As for the aluminium, almost the entire life is occupied by the gradual advancement of the crack across the minimum section. In figure 18 the stress distributions are given for 316 stainless steel. The first crack, or failure, occurs after 0.0147 % of life, after which time the spatial distributions are similar to the equivalent extrapolated stationary-state distribution,  $n = 1.74$ , obtained by Hayhurst & Henderson (1977). After 4.43 % of life the crack has advanced across the minimum section to a distance  $\bar{r} = 0.92$ , thereafter the crack growth is predominantly away from the  $r$ -axis.

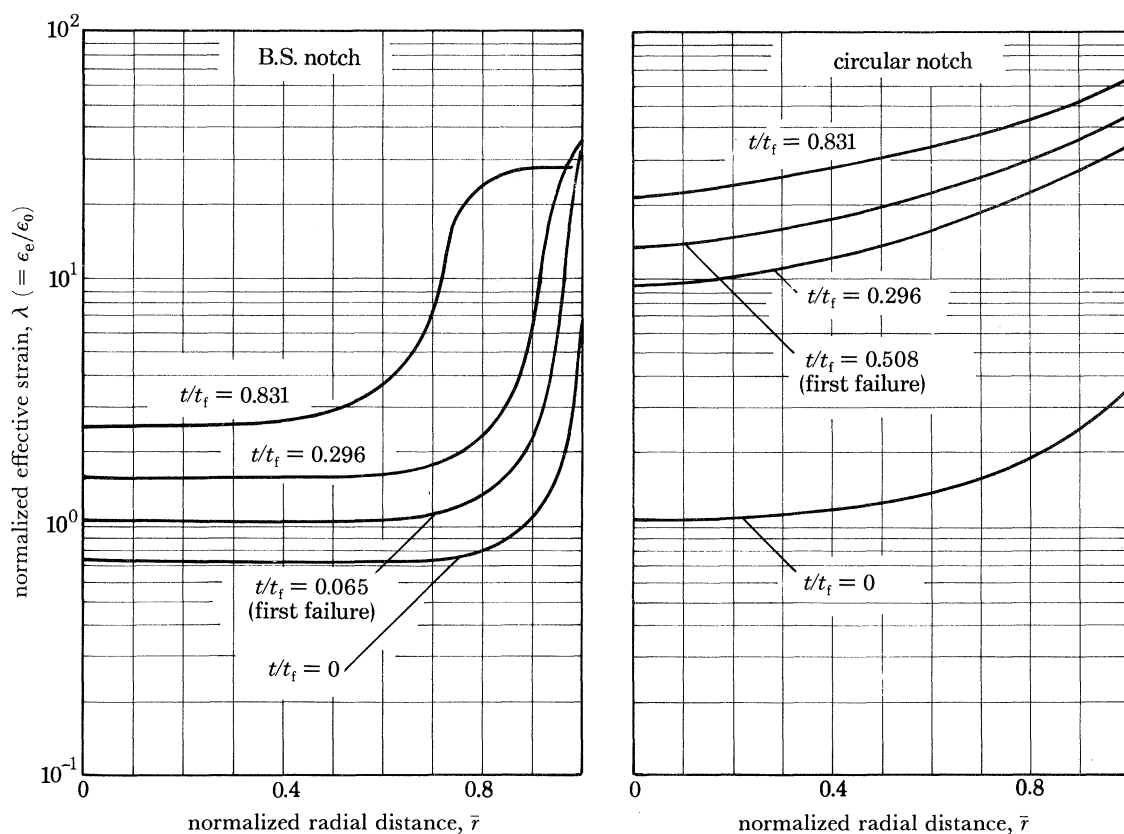


FIGURE 19. The change of the effective strain variation across the minimum section of the notch ( $z = 0$ ) with the normalized time  $t/t_f$  in the circular and B.S. notches for copper.

## 5. DISCUSSION

The validity of the approximate solutions due to Hayhurst *et al.* (1978), which are based on stationary-state solutions and the assumption of kinematical determinacy, can be assessed by using the present solutions. In figure 19 the variations of the normalized effective strain

$$\lambda_e = \left( \frac{2}{3} \epsilon_{ij} \epsilon_{ij} \right)^{1/2} / \epsilon_0$$

with normalized radial distance  $\bar{r}$  are given for different values of  $t/t_f$ . The curves for the circular notch in copper may be described by

$$\lambda_e = [H \pm (0.15H)] \lambda_c^{e1}, \quad (20)$$



where  $\lambda_e^{e1}$  is the normalized elastic effective strain at  $t/t_f = 0$  and the value of  $H$  ranges from 10.4 to 20.6 for the curves shown in figure 19. This description is slightly better than that reported by Hayhurst *et al.* (1978). The description for copper is typical of that for aluminium, but (20) describes the behaviour of the circular notch in 316 stainless steel less well because first failure takes place early in the lifetime and effectively reduces the minimum section. It would appear that the assumption of kinematical determinacy is a good one for situations, in circular notches, where the first crack forms relatively late in the lifetime. For situations where this is not the case simplifications based on kinematical determinacy are inappropriate and a full time-iterative solution is required instead. The assumption of kinematical determinacy for the B.S. notch in copper may be seen from figure 19 to be less good, for this specimen the behaviour of copper is typical of that for the aluminium alloy and for 316 stainless steel. The solutions due to Hayhurst *et al.* (1978) based on kinematically determinate behaviour are obviously not totally accurate. The normalized times for first failure were  $t/t_f = 0.99580$  and  $t/t_f = 0.428$  for the aluminium alloy and copper respectively, these results compare with the values,  $t/t_f = 0.024$  and  $t/t_f = 0.065$  respectively, obtained for the time-iterative solutions. The reasonably good agreement between the values of  $\Sigma_r$ , determined experimentally and by using the kinematically determinate solution procedure must, in part, be fortuitous.

The numerical solutions for the circular notches, in the aluminium alloy, in copper, and to a lesser extent in 316 stainless steel, show that a significant volume of material at the minimum section of the notch is subjected to multi-axial states of stress with a high value of  $J_1/\sigma_{ii}$  for a relatively long period of time. For all three materials the time-iterative solution may be used, in conjunction with the results of experiments and uni-axial data, to determine a value of  $\alpha$ , or the multi-axial stress rupture criterion, for the material. This approach has considerable appeal since a circular notch specimen can be tested in the same machine as an un-notched uni-axial specimen and so avoids the complexities of multi-axial testing machines and specimens.

Two distinct features emerge on comparison of the results of circular and B.S. notches: first, that the circular notch shows characteristics of a specimen that is damaged uniformly in the region of the minimum section and in which failure takes place relatively uniformly towards the end of the life, as, for example, in an un-notched uni-axial specimen; second, that in the case of the B.S. notch the first crack forms early in the lifetime and propagates relatively slowly across the specimen. The latter situation is well removed from the type of behaviour found in the homogeneously stressed region of the circular notch; the extent of the regions of high damage is confined to the close proximity of the crack and the behaviour is similar to that for the growth of a crack due to creep in a slightly damaged continuum. This observation is of interest since it suggests that the continuum damage process, used by the solution procedure described in this paper, is probably the mechanism by which well-defined cracks grow by creep.

Two observations are of particular interest in the growth of damage in the B.S. notches: first, in the aluminium solution the zones of damage form in the regions of the shear lobes yet the crack propagates along the  $r$ -axis; second, in the stainless steel solution the zones of damage and the crack both develop in the same direction, away from the  $r$ -axis. It is of interest to ascertain what are the features of the stress states and their changes in time which result in these effects. With this aim in mind contours of stress and damage states have been plotted in figures 20 and 21 for the region of the minimum section of the notch at two different times for the aluminium alloy and for the 316 stainless steel. The dark shaded regions in the finite element mesh denote the current locations of the crack. In the case of the aluminium alloy (figure 20) the regions of high shear,

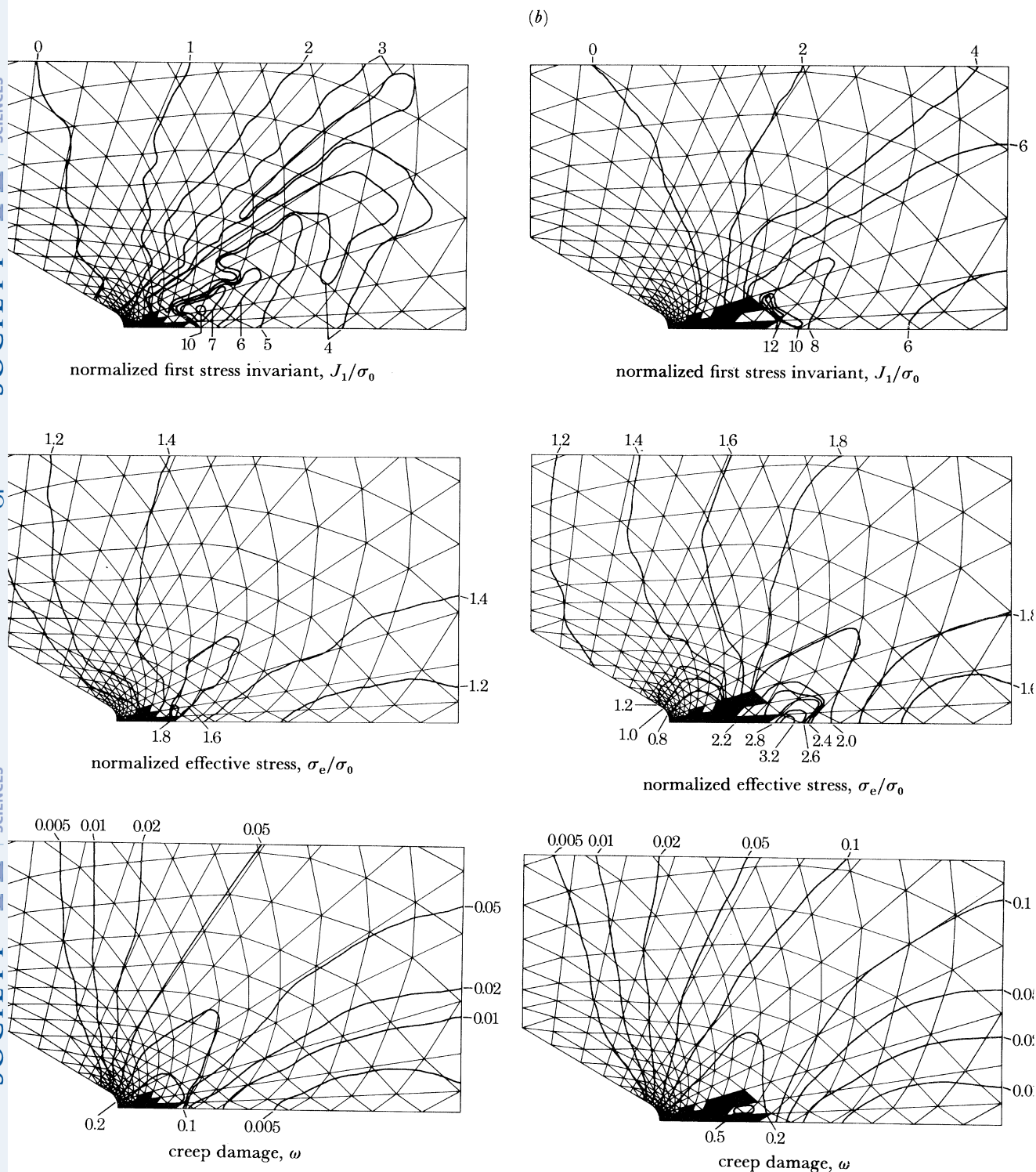


FIGURE 20. Contours of constant stress and damage for a B.S. notched aluminium alloy bar at (a)  $t/t_f = 0.76$  and (b)  $t/t_f = 0.97$ .

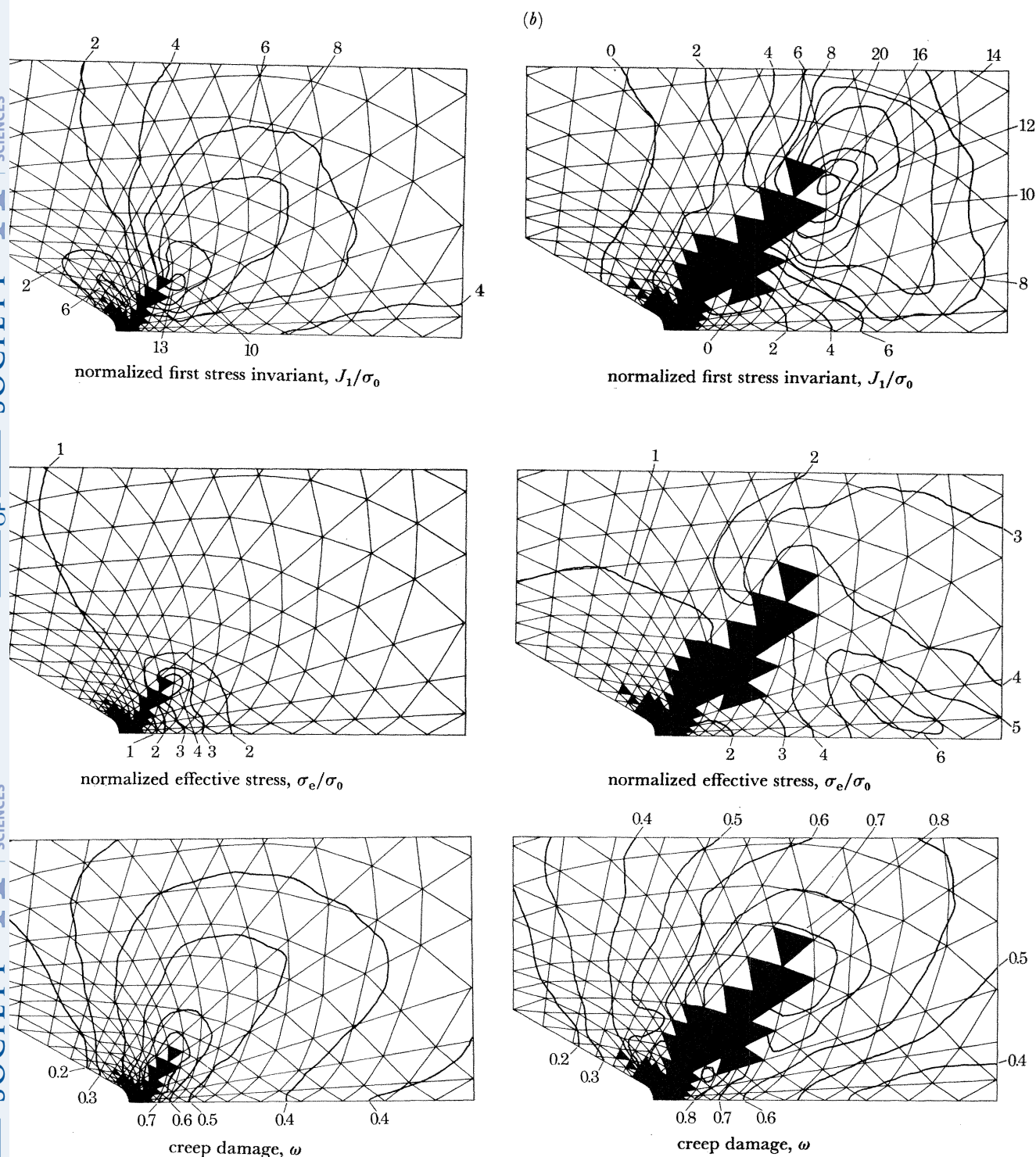


FIGURE 21. Contours of constant stress and damage for a B.S. notched 316 stainless steel bar at (a)  $t/t_f = 0.044$  and at (b)  $t/t_f = 0.51$ .

THE ROYAL SOCIETY OF MATHEMATICAL, PHYSICAL & ENGINEERING SCIENCES  
 PHILOSOPHICAL TRANSACTIONS OF THE ROYAL SOCIETY OF MATHEMATICAL, PHYSICAL & ENGINEERING SCIENCES

$\sigma_e/\sigma_0$ , can be seen to remain on the  $r$ -axis and in the shear lobes for  $t/t_f = 0.76$  and  $0.97$ . The same features can be seen in the distributions of damage, since  $\alpha = 0$  or aluminium alloys satisfy a maximum  $\sigma_e/\sigma_0$  rupture criterion, except that as the crack moves forward it carries with it the distribution of  $\sigma_e/\sigma_0$  and hence tends to smear the damage over the region through which the shear lobes pass. The distributions of the normalized first stress invariant show that a zone of maximum  $J_1/\sigma_0$  remains ahead and slightly above the crack tip as it moves. This region, remains in a zone of high damage but suppresses the growth of further damage since  $\sigma_e/\sigma_0$  is maintained low in the region. Hence the crack moves forward along the  $r$ -axis.

Similar plots are presented in figure 21 for a B.S. notch in 316 stainless steel at the normalized times  $t/t_f = 0.044$  and  $0.51$ . The distribution of  $\sigma_e/\sigma_0$  show that the highest values occur in the region between the crack and the  $r$ -axis at both times. As in the situation for the aluminium alloy the maximum value of the normalized first stress invariant,  $J_1/\sigma_0$ , occurs at the tip of the crack and, in this case, slightly below it. The distribution of the maximum principal tension stress is very similar to that for the normalized first stress invariant and is not presented here. Since 316 stainless steel obeys predominantly a maximum principal tension stress rupture criterion damage occurs ahead of the crack in the  $J_1/\sigma_0$  field, where the field is most intensely damaged.

The manner in which the cracks propagate in the notches appears to be dependent upon three factors:

- (i) the multi-axial stress rupture criterion of the material;
- (ii) the geometry and loading of the specimen and the initial stress fields that they produce;
- (iii) the time dependent interaction between the multi-axial character of the stress fields and the multi-axial rupture behaviour of the material.

One would expect these effects to be most pronounced in structural members that contain sharp cracks where conditions of high constraint are known to exist (Hayhurst & Brown 1984).

## 6. CONCLUSIONS

A numerical method for the solution of boundary value problems, in which continuum damage is allowed to develop and to change the boundary of the body in a time-dependent manner, has been described and used to predict representative rupture stresses for circular and B.S. notched specimen in three materials. Damage fields have been predicted and shown to be in close agreement with the results of metallographic studies.

The numerical solutions for both the circular and B.S. notches have been used in conjunction with the results of experiments to establish the  $\alpha$ -value or the multi-axial stress rupture criteria for the three materials examined; the value of  $\alpha = 0$  has been confirmed for the aluminium alloy and values  $\alpha = 0.7$  and  $0.75$  have been obtained for copper and 316 stainless steel respectively.

The approximate solutions due to Hayhurst *et al.* (1978) obtained for circular B.S. notches using stationary-state solutions and assuming kinematical determinacy of the minimum sections of the notches are invalid for the B.S. notch, but valid for the circular notch with materials in which cracking does not take place early in life; those materials for which  $n$  and  $\chi$  are high appear to fall into this category.

The numerical solutions show that, for the circular notch with material for which  $n$  is large, the stresses redistribute close to the stationary-state values without the formation of pronounced damage. Under these circumstances rupture takes place uniformly as in a homogeneously stressed specimen, and the specimen may be used in conjunction with the stationary-state



solutions (Hayhurst & Henderson 1977), as shown by Dyson & Loveday (1981) and by Needham & Gladman (1980), to test materials under multi-axial states of stress and to determine the  $\alpha$ -value or the multi-axial stress rupture criterion of the material. The aluminium alloy and copper appear to fall into this category but in the case of 316 stainless steel the usage of the stationary-state distributions is inappropriate since local damage forms at an early stage and it is necessary to use the time-iterative solution to obtain the value of  $\alpha$ . Graphs such as those presented in figures 4 and 5 are helpful in these circumstances.

Comparison of the numerical results for the circular and for B.S. notches shows that for the circular notch, large volumes of material are subjected to homogeneous stress states for relatively long periods of time. This is in contrast with the behaviour of the B.S. notch in which high stress gradients are found and damage is confined to small regions of material. As a result small, crack-like zones of damaged material form and propagate. This observation is evidence that the theory of continuum damage mechanics may be capable of predicting the formation and propagation of discrete cracks.

Several people have contributed to the work reported here; in particular, the authors wish to express their gratitude to J. T. Henderson, A. J. Krzeczowski and P. R. Brown.

#### APPENDIX. TIME INTEGRATION PROCEDURE

##### A 1. *Integration of creep strains and damage*

The procedure used is the fourth order Runge–Kutta method described by Hayhurst & Henderson (1977). At any time  $\tau$  the rate of change of a component of creep strain  $V_{ij}^s$  can be written

$$dV_{ij}^s/d\tau = f^s(V_{ij}^s, \omega^s, \tau), \quad (\text{A } 1)$$

where  $V_{ij}^s$  and  $\omega^s$  are the creep strain and damage at time  $\tau$  respectively and  $f^s$  is a function dependent upon the boundary value problem. In the same way the rate of change of damage may be expressed by

$$d\omega^s/d\tau = g^s(V_{ij}^s, \omega^s, \tau), \quad (\text{A } 2)$$

where  $g^s$  has a similar interpretation to  $f^s$ . If one is to use the Runge–Kutta method which is based on (A 1) and (A 2) then difficulties may be encountered with the change in the value of  $\omega(\tau)$  over the time step  $\Delta\tau$ . If the value of  $\omega$  in a material element exceeds unity then the corresponding rate equations are invalidated. It is possible to arrange for the inequalities  $0 < \omega \leq 1$  to be satisfied over any time step, but the level of computational efficiency suffers as a result. This difficulty was overcome by assuming that  $\omega^s$  in (A 1) and (A 2) remains constant at its starting value for a particular time step. It may be argued that this approach is valid provided that the integration steps are maintained sufficiently small to ensure that the errors in the integration of damage are acceptable. Procedures that have been developed to control both time step and integration error are described in a later section.

With these provisos (A 1) and (A 2) may be rewritten as

$$dV_{ij}^s/d\tau = \dot{V}_{ij}^s = f^s(V_{ij}^s, \hat{\omega}, \tau),$$

and

$$d\omega^s/d\tau = \dot{\omega}^s = g^s(V_{ij}^s, \hat{\omega}, \tau),$$



where  $\hat{\omega}$  is the damage value at the start of an integration step. The creep strain rates  $\dot{V}_{ij}^s$  at the time  $\tau + \Delta\tau$  are obtained by using the following algorithm:

$$\left. \begin{aligned} \dot{V}_{ij}^{s1} &= f^s(V_{ij}^s(\tau), \hat{\omega}, \tau), \\ \dot{V}_{ij}^{s2} &= f^s(V_{ij}^s(\tau) + \frac{1}{3}\Delta\tau \dot{V}_{ij}^{s1}, \hat{\omega}, (\tau + \frac{1}{3}\Delta\tau)), \\ \dot{V}_{ij}^{s3} &= f^s(V_{ij}^s(\tau) + \frac{1}{6}\Delta\tau \dot{V}_{ij}^{s1} + \frac{1}{6}\Delta\tau \dot{V}_{ij}^{s2}, \hat{\omega}, (\tau + \frac{1}{2}\Delta\tau)), \\ \dot{V}_{ij}^{s4} &= f^s(V_{ij}^s(\tau) + \frac{1}{8}\Delta\tau \dot{V}_{ij}^{s1} + \frac{3}{8}\Delta\tau \dot{V}_{ij}^{s3}, \hat{\omega}, (\tau + \frac{3}{4}\Delta\tau)), \\ \dot{V}_{ij}^{s5} &= f^s(V_{ij}^s(\tau) + \frac{1}{2}\Delta\tau \dot{V}_{ij}^{s1} - \frac{3}{2}\Delta\tau \dot{V}_{ij}^{s3} + 2\Delta\tau \dot{V}_{ij}^{s4}, \hat{\omega}, (\tau + \Delta\tau)), \\ \dot{V}_{ij}^s &= \{V_{ij}^s(\tau) + \frac{1}{6}\Delta\tau \dot{V}_{ij}^{s1} + \frac{2}{3}\Delta\tau \dot{V}_{ij}^{s4} + \frac{1}{6}\Delta\tau \dot{V}_{ij}^{s5}\}, \end{aligned} \right\} \quad (\text{A } 3)$$

and the error term by

$$\Delta V_{ij}^{se} = \frac{1}{30}(2\Delta\tau \dot{V}_{ij}^{s1} - 9\Delta\tau \dot{V}_{ij}^{s3} + 8\Delta\tau \dot{V}_{ij}^{s4} - \Delta\tau \dot{V}_{ij}^{s5}). \quad (\text{A } 4)$$

Similar equations for the damage integration algorithm may be obtained by replacing  $\dot{V}$  by  $\dot{\omega}$  and  $V$  by  $\omega$  in the above equations; hence the corresponding equation to (A 3) then becomes

$$\omega^s = \{\omega^s(\tau) + \frac{1}{6}\Delta\tau \dot{\omega}^{s1} + \frac{2}{3}\Delta\tau \dot{\omega}^{s4} + \frac{1}{6}\Delta\tau \dot{\omega}^{s5}\}. \quad (\text{A } 5)$$

The functions  $f^s$  and  $g^s$  refer to the solution of the creep problem for given creep strain and damage fields; the corresponding rate fields are then determined from the constitutive equations by using the appropriate stress fields.

## A 2. Selection of time-step

A number of problems were encountered in the selection of the time-step. First, when creep strains and damage values were small the normal controls on these variables were inappropriate. For this situation an overall force equilibrium check was used which previous experience had shown to be sensitive to the size of the time-step. Second, the relative and absolute changes in damage over any time-step had to be controlled, for the reasons discussed earlier. Somewhat arbitrary limits were set after experimentation. Finally, the relative and absolute errors in the integration of creep strains had to be controlled within close limits since the problems under investigation required several hundred integration steps. The different time-step controls employed are now discussed in turn.

### A 2.1. Selection of first time-step

The Runge–Kutta procedure requires the specification of a time-step which defines the interval over which integration is to be carried out, the start of the interval being the current time.

The first time-step was selected in an arbitrary manner. After integration over this time-step an accuracy check was carried out by using the following integral

$$\int_{A_m} (\sigma_{zz}/\sigma_0) dA = \hat{P}/\sigma_0,$$

where  $\sigma_{zz}/\sigma_0$  is the normalized component of stress in the direction of the applied load  $P$  and  $A_m$  is the minimum area ( $z = 0$ ), normal to the direction of  $P$ . The value of  $\hat{P}$  will differ from  $P$  by an error  $R = |\hat{P}/P - 1|$ . If both of the following inequalities,

$$R_2 > R_1, \quad \text{and} \quad |R_1 - R_2| > 0.001 R_1, \quad (\text{A } 6)$$

where  $R_1$  is the value corresponding to the elastic solution and  $R_2$  is the value after the first integration step, were satisfied then the integration was repeated with the time-step reduced to one tenth of its previous value. If the inequalities were still satisfied then the procedure was repeated until the conditions expressed in (A 6) were violated.

### A 2.2. Selection of subsequent time-steps

On the first attempt at integration from a time  $\tau$  over a time-step  $\Delta\tau$ , the selection of the interval of integration was based on the three following considerations:

- (i) a value predicted from the previous time-step,  $\Delta\tau_p$ , with techniques to be described later;
- (ii) a value based on the increase in the absolute damage, and determined by,

$$\Delta\tau_a = 0.1/\dot{\omega}_{\text{amax}},$$

where  $\dot{\omega}_{\text{amax}}$  is the maximum damage rate considered throughout the volume of the structure for which  $\omega < 0.8$ ;

- (iii) a value based on the increase in the relative damage, and determined by,

$$\Delta\tau_r = 0.05/\omega_{\text{rmax}},$$

where  $\omega_{\text{rmax}} = \max |\dot{\omega}/\omega|$  over those elements for which  $\omega \geq 0.8$ . The time-step was selected by

$$\delta = \min[\Delta\tau_p, \Delta\tau_a, \Delta\tau_r] \quad (\text{A } 7)$$

with the two following exceptions:

- (i) if the integration step was the first or the first after an element had failed, then  $\Delta\tau_p$  was omitted from the above equation;
- (ii) if no element had a damage value greater than 0.8 then  $\Delta\tau_r$  was omitted.

### A 2.3. Criteria for acceptance of selected time-step

The time-step was accepted provided that the error  $e_{ij}^s = \Delta V_{ij}^{s0}(\tau + \Delta\tau)$  determined from (A 4), for all components of creep strain satisfy certain criteria. The main criterion used is defined by

$$|e_{ij}^s/V_{ij}^s| < 0.001. \quad (\text{A } 8)$$

To overcome the difficulties that arise when  $V_{ij}^s$  are small, a subsidiary criterion is defined by

$$|e_{ij}^s/\bar{V}| < 0.001, \quad (\text{A } 9)$$

where  $\bar{V}$  is some value of the mean value of the absolute creep strain given by

$$\bar{V} = \frac{0.01}{4q} \sum_{s=1}^{s=q} \sum_1^4 |V_{ij}^s|,$$

$q$  is the number of unfailed elements and where the inner summation is carried out for the four components of stress within an element and is used whenever

$$|V_{ij}^s| < \bar{V}. \quad (\text{A } 10)$$

Error estimates for each creep strain component within the field were computed from (A 4) and checked against the criteria given by (A 8) and (A 9). The maximum error for both criteria was determined for those creep strain components which do not satisfy the criteria. If all components satisfy the appropriate criterion then the integration proceeded to the next time-step, but if the error criteria were violated then the integration step was repeated with a successively smaller time-step until the criterion was satisfied.

The procedure used is summarized below.

- (1) To prevent the possibility of oscillation in time-step the acceptable ranges used for the criteria were

$$[|e_{ij}^s/V_{ij}^s|/0.001] \leq 1.0 \quad \text{for (A 8),}$$

$$[|e_{ij}^s/V|/0.001] \leq 1.1 \quad \text{for (A 9).}$$

The criterion (A 8) was checked first.

- (2) If (A 8) was satisfied, but not (A 9), then the integration step was repeated with a time-step equal to one half of the previous value. The value of one half was decided after experiment with a range of values.
- (3) If (A 8) was not satisfied then the time-step was reduced by the factor  $\Theta$ , where

$$\Theta = [|e_{ij}^s/V_{ij}^s|_{\max}/0.001]^{-0.2},$$

for  $\Theta$  in the range  $0.1 > \Theta > 0.9$ , if  $\Theta$  was outside these limits then it was set to the limit violated, and the integration step repeated.

- (4) If the errors associated with all strain components within the body did not violate the appropriate criterion then for the next iteration the time-step was multiplied by the factor  $\Theta$  for  $2 > \Theta > 1.1$ , and by a factor of 2 for  $\Theta \geq 2$ , or if  $\Theta \leq 1.1$  then the previous time-step was used.

Some of the control variables were somewhat arbitrarily selected but the integration process was carried out satisfactorily and far more accurately and rapidly than with the Euler method.

## REFERENCES

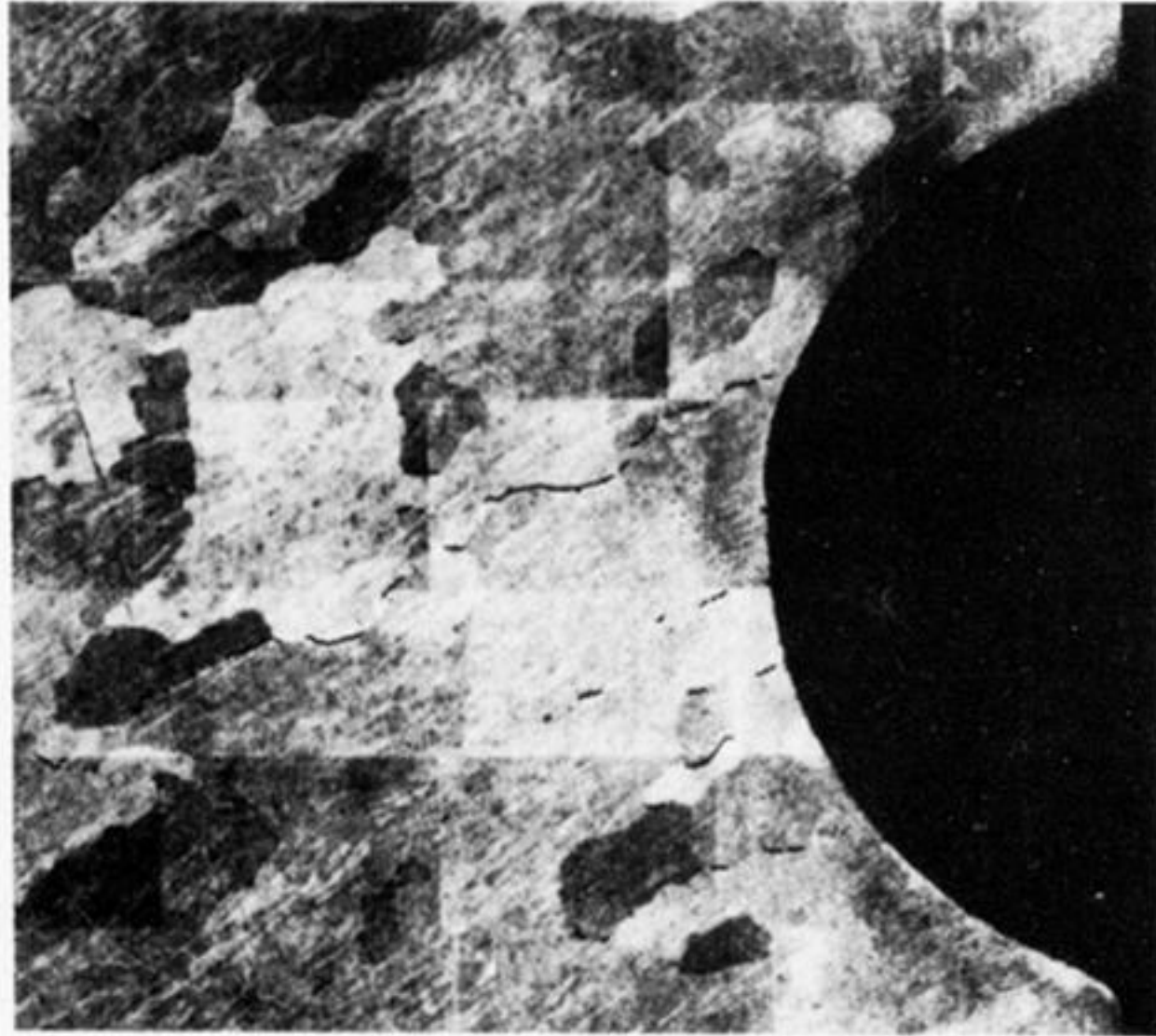
- American Society for Mechanical Engineers 1977 code case N47. Interpretations of A.S.M.E. boiler and pressure vessel code.
- Ashby, M. F. 1972 A first report on deformation-mechanism maps. *Acta metall.* **20**, 887.
- Bridgman, P. W. 1952 *Studies in large plastic flow and fracture*. New York: McGraw-Hill.
- British Standards 1969 no. 3500, part 1. Methods for creep rupture testing of metals.
- British Standard 1982 no. 5500. Specification for unfired fusion welded pressure vessels.
- Chubb, E. J. & Bolton, C. J. 1980 Stress state dependence of creep deformation and fracture in AISI type 316 stainless steel. *Proc. Int. Conf. on Engng aspects of Creep*, 15–19 Sept. 1980 *Sheffield*, **1**, paper C201/80, p. 48. London: Institute of Mechanical Engineers.
- Dyson, B. F. & Loveday, M. 1981 Creep fracture in Nimonic 80A under triaxial tensile stressing. *Creep in structures*, 1980 (*I.U.T.A.M. Symposium, Leicester, U.K.*) (ed. A. R. S. Ponter & D. R. Hayhurst), p. 406. Berlin: Springer-Verlag.
- Dyson, B. F. & McLean, D. 1977 Creep of Nimonic 80A in torsion and tension. *Metal Sci. J.* **11**, 37.
- Greenwood, G. 1973 Creep life and ductility. *Int. Conf. on Metals, Cambridge*. Micro-structure and the design of alloys, **2**, 91.
- Hayhurst, D. R. 1970 Isothermal creep deformation and rupture of structures. Ph.D. thesis, Cambridge University.
- Hayhurst, D. R. 1972 Creep rupture under multi-axial states of stress. *J. Mech. Phys. Solids* **20**, 381.
- Hayhurst, D. R. 1973 Stress redistribution and rupture due to creep in a uniformly stretched thin plate containing a circular hole. *J. appl. Mech.* **40**, 244.
- Hayhurst, D. R. 1979 Recent developments in high temperature design methods. *Chartered Mechanical Engineer*, **26**, 73.
- Hayhurst, D. R. & Brown, P. R. 1984 The use of finite element creep solutions to obtain  $J$  integrals for plane strain cracked members. *Int. J. mech. Sci.* **26**, 29.
- Hayhurst, D. R., Dimmer, P. R. & Chernuka, M. W. 1975 Estimates of the creep rupture lifetime of structures using the finite element method. *J. Mech. Phys. Solids* **23**, 335.
- Hayhurst, D. R. & Henderson, J. T. 1977 Creep stress redistribution in notched bars. *Int. J. mech. Sci.* **19**, 133.
- Hayhurst, D. R. & Krzczkowski, A. J. 1979 Numerical solution of creep problems. *Comput. Meth. appl. Mech. Engng* **20**, 151.

## CREEP RUPTURE OF NOTCHED BARS

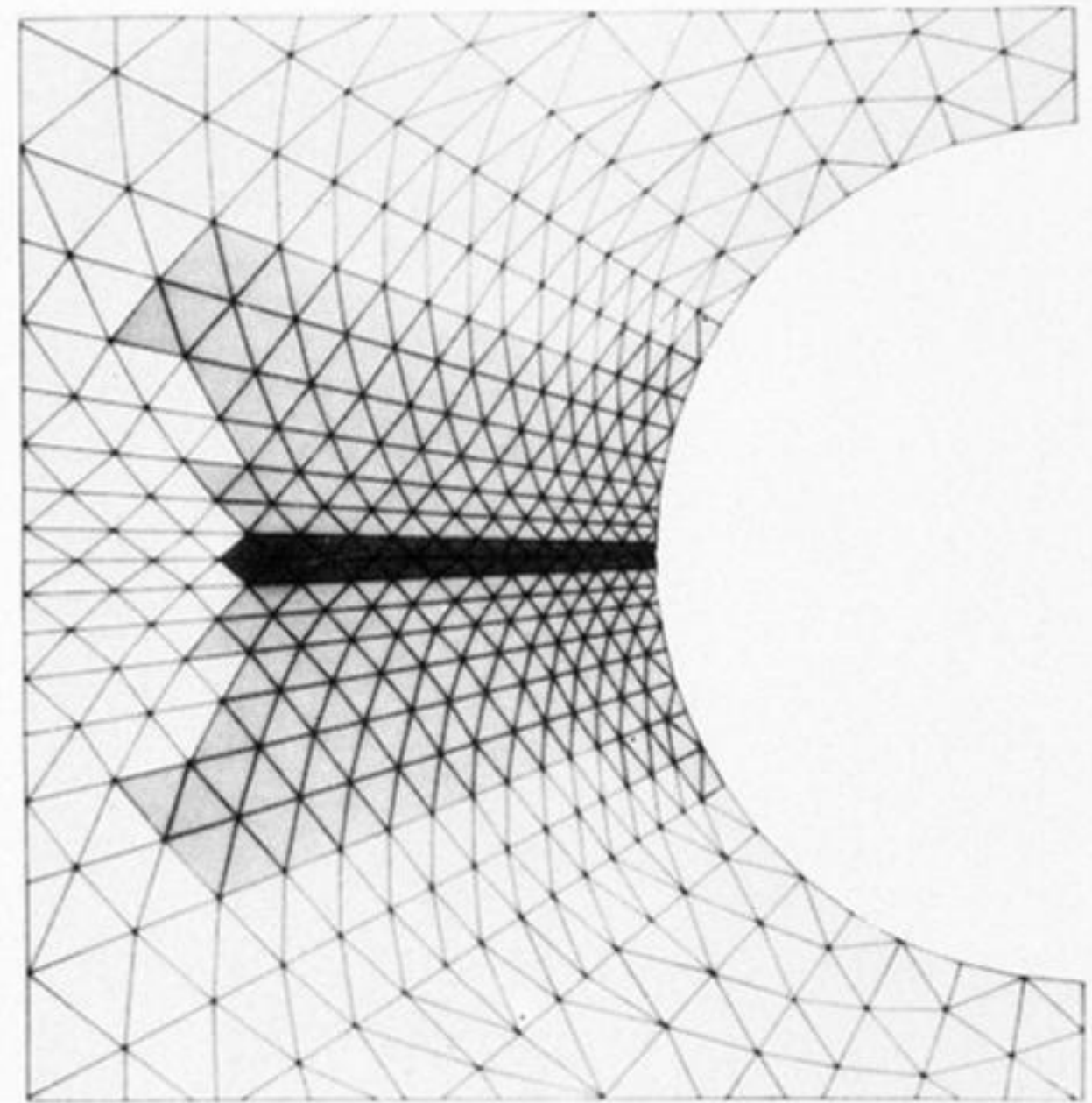
129


- Hayhurst, D. R. & Leckie, F. A. 1973 The effect of creep constitutive and damage relationships upon the rupture time of a solid circular torsion bar. *J. Mech. Phys. Solids* **21**, 431.
- Hayhurst, D. R., Leckie, F. A. & Morrison, C. J. 1978 Creep rupture of notched bars. *Proc. R. Soc. Lond. A* **360**, 243.
- Hayhurst, D. R., Morrison, C. J. & Brown, P. R. 1981 Creep crack growth. *Creep in structures*, 1980 (*I.U.T.A.M. Symposium, Leicester, U.K.*) (ed. A. R. S. Ponter & D. R. Hayhurst), p. 564. Berlin: Springer-Verlag.
- Hayhurst, D. R. & Storåkers, B. 1976 Creep rupture of the Andrade shear disk. *Proc. R. Soc. Lond. A* **349**, 369.
- Hayhurst, D. R., Trampczynski, W. A. & Leckie, F. A. 1983 On the rôle of cavity nucleation in creep deformation and fracture. *Acta metall.* **31**, 1537.
- Johnson, A. E., Henderson, J. & Khan, B. 1962 Complex-stress creep, relaxation and fracture of metallic alloys. Edinburgh: H.M. Stationery Office.
- Kachanov, L. M. 1958 Time of the fracture process under creep conditions. *Izv. Akad. Nauk SSSR Otd. Teck. Nauk* **8**, 26.
- Leckie, F. A. & Hayhurst, D. R. 1974 Creep rupture of structures. *Proc. R. Soc. Lond. A* **340**, 323.
- Leckie, F. A. & Hayhurst, D. R. 1977 Constitutive equations for creep rupture. *Acta metall.* **25**, 1059.
- Loveday, M. S. & Dyson, B. F. 1979 Creep deformation and cavitation damage in Nimonic 80A under triaxial tensile stress. *Proc. I.C.M.* **3**, 2, 213 (*Mechanical behaviour of materials*) (ed. K. J. Miller & R. F. Smith). Oxford: Pergamon.
- Morrison, C. J. 1976 Creep rupture of cylindrical notched bars. M.Phil. thesis, Leicester University.
- Needham, N. G. & Gladman, T. 1980 The effect of stress-state on the processes controlling creep fracture in 2½% Cr 1% Mo steel. *Proc. Int. Conf. on Engng aspects of Creep*, 15–19 Sept. 1980, *Sheffield*, **1**, paper C190/80, p. 49. London: Institute of Mechanical Engineers.
- Odqvist, F. K. G. 1974 *Mathematical theory of creep and creep rupture*, 2nd edn, ch. 12. Oxford: Clarendon Press.
- Odqvist, F. K. G. & Hult, J. 1961 Some aspects of creep rupture. *Ark. Fys.* **19**, 379.
- Penny, R. K. & Hayhurst, D. R. 1969 The deformations and stresses in a stretched thin plate containing a hole during stress redistribution caused by creep. *Int. J. mech. Sci.* **11**, 23.
- Robinson, E. L. 1952 Effect of temperature variation on the long-time rupture strength of steels. *Trans. Am. Soc. mech. Engrs* **74**, 777.
- Trampczynski, W. A., Hayhurst, D. R. & Leckie, F. A. 1981 Creep rupture of copper and aluminium under non-proportional loading. *J. Mech. Phys. Solids* **29**, no. 5/6, 353.





aluminium



  $\omega \geq 0.99$


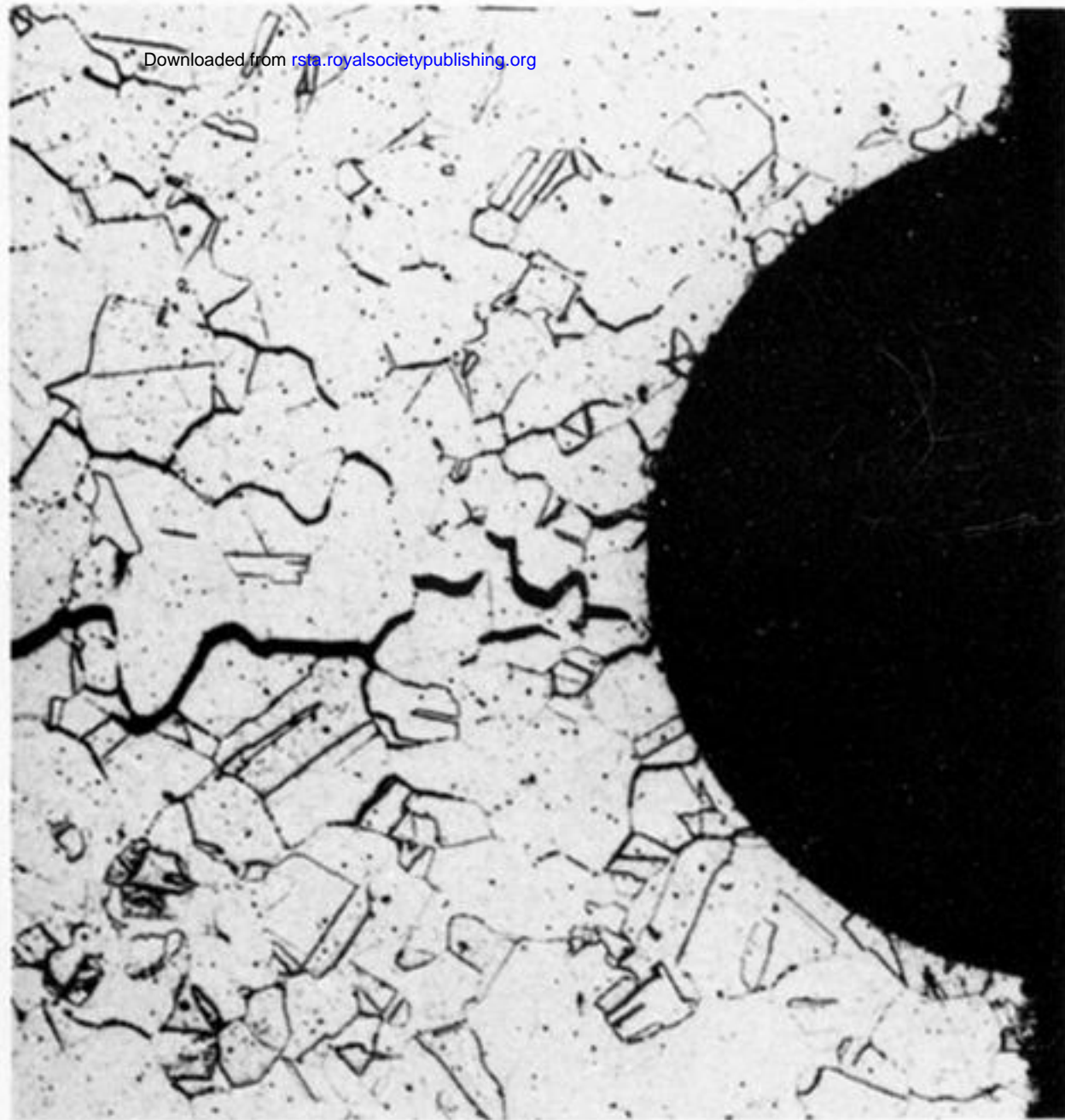
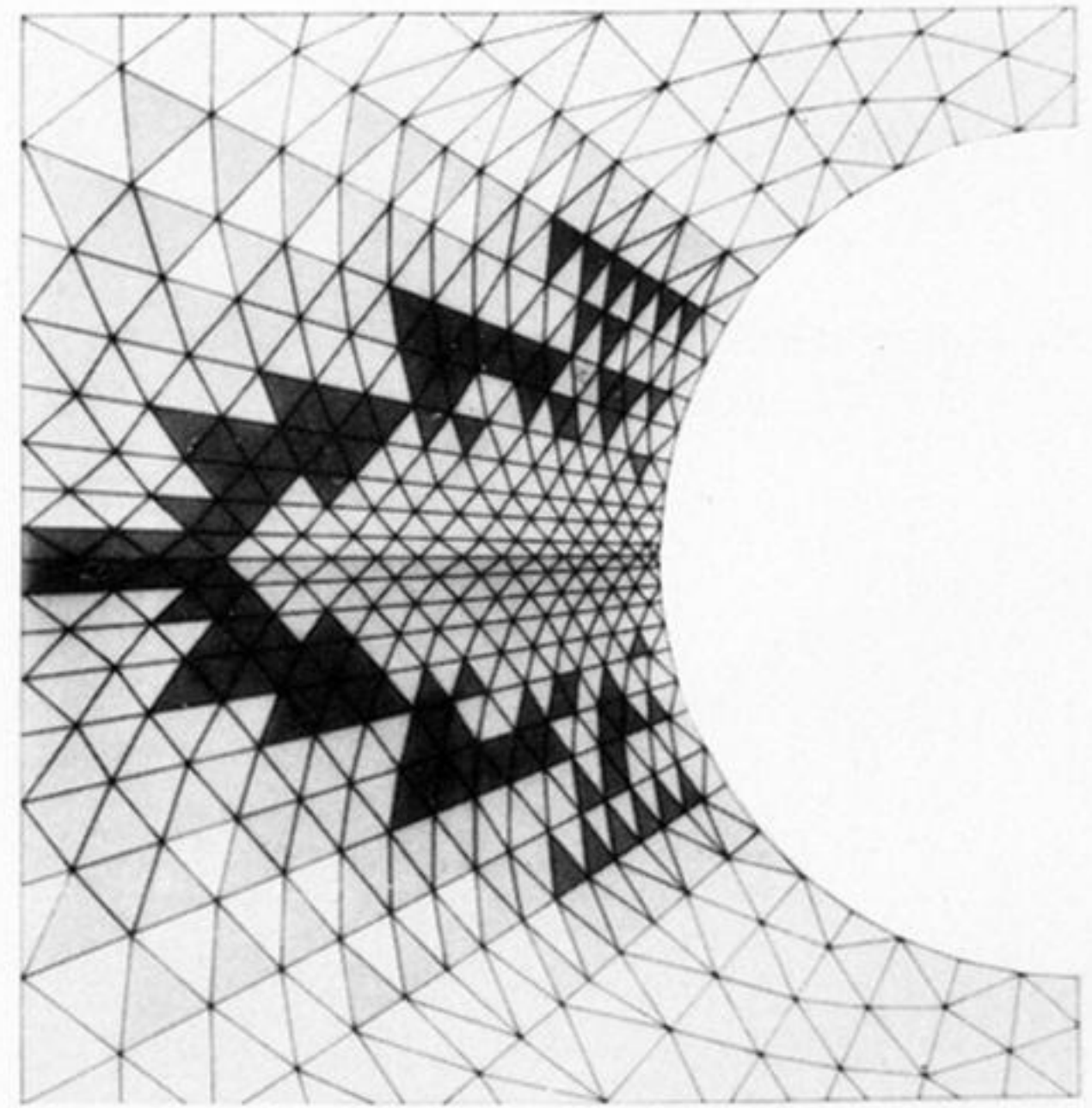
  $\omega \geq 0.10$


FIGURE 7. Comparison of a theoretical prediction of the distribution of damage in a circular notched bar with that observed in a micrograph taken from a diametral plane close to failure.





copper



  $\omega \geq 0.99$


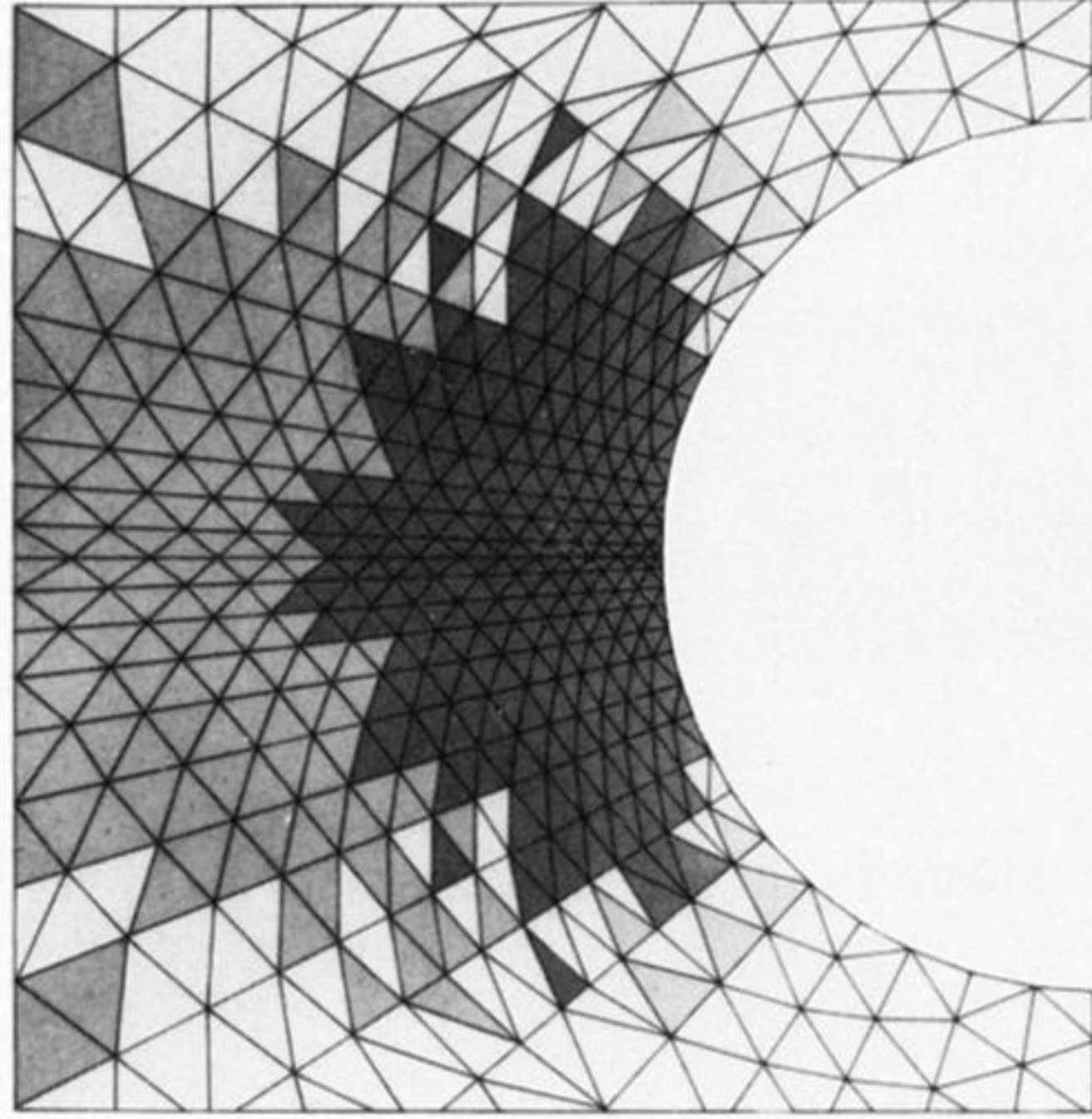
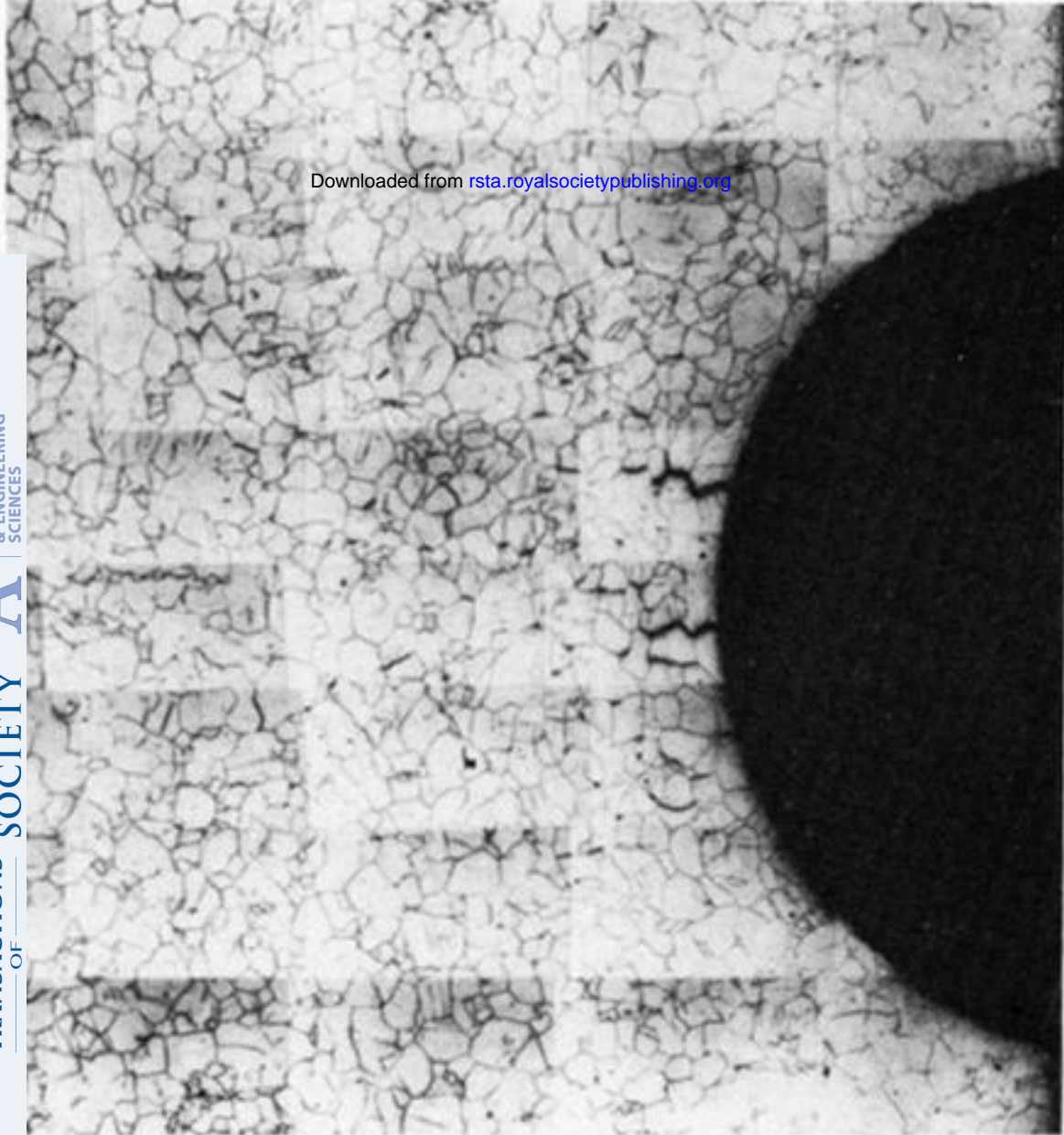


  $\omega \geq 0.10$

FIGURE 8. Comparison of a theoretical prediction of the distribution of damage in a circular notched bar with that observed in a micrograph taken from a diametral plane close to failure.





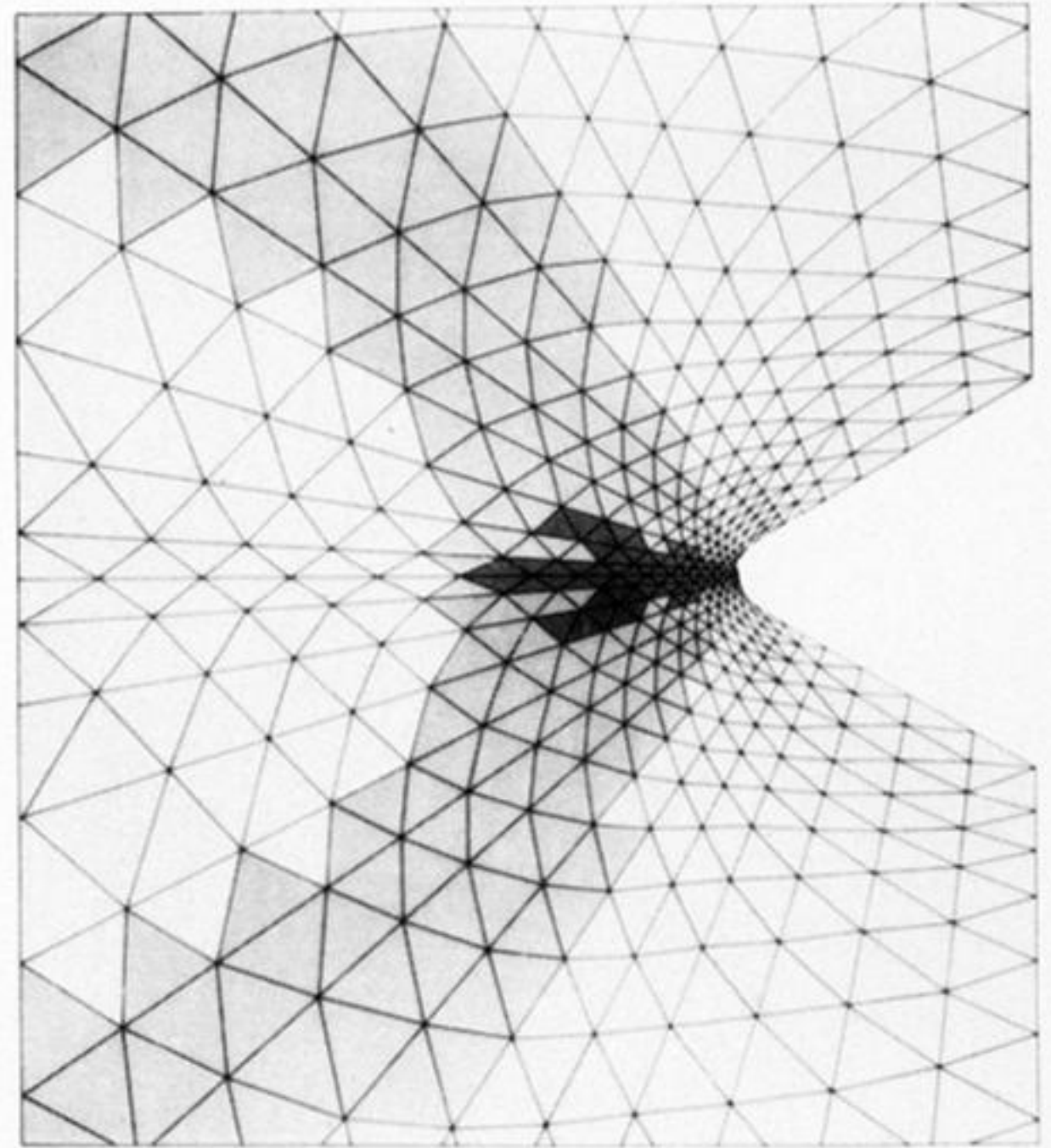
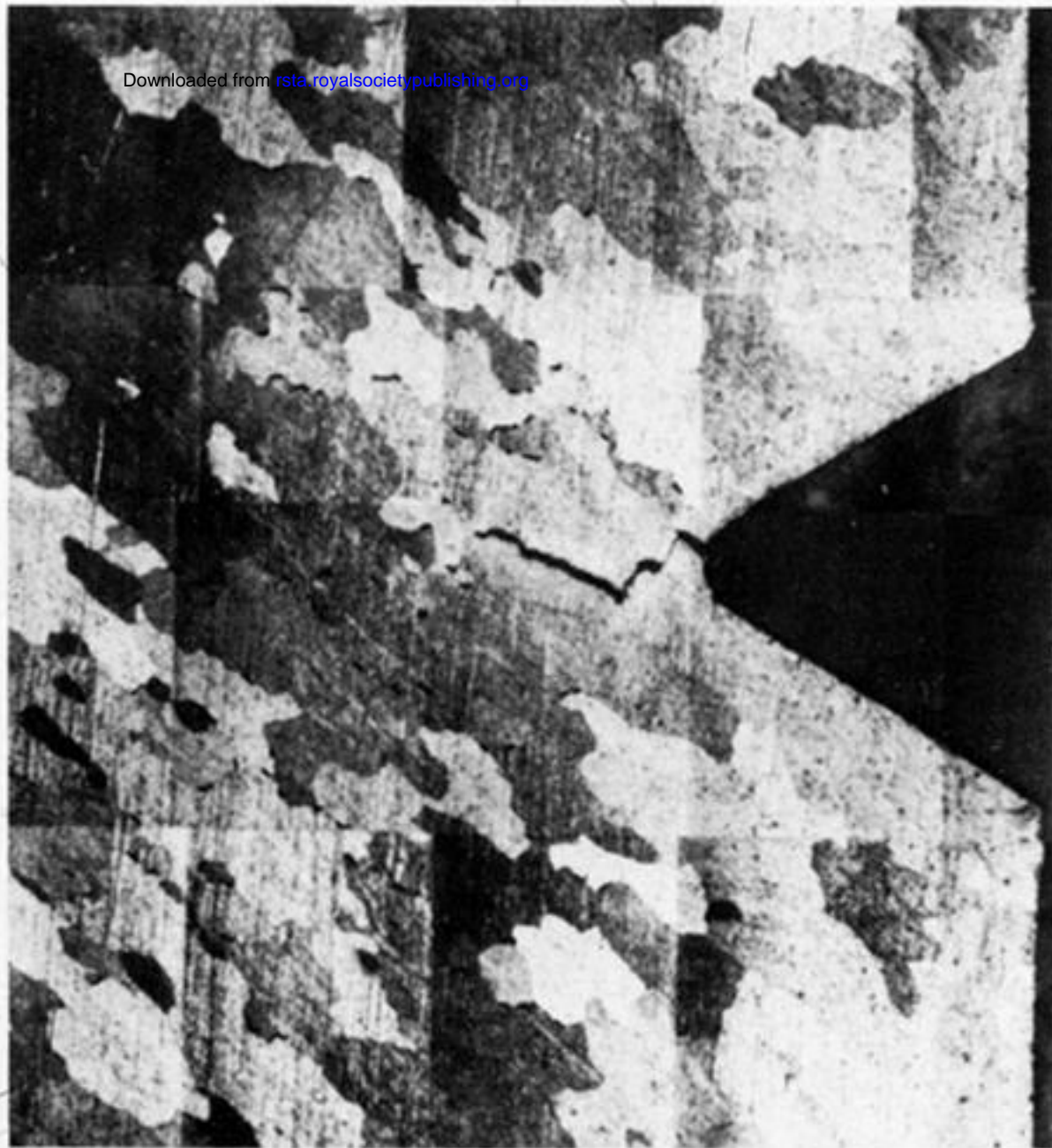
  $\omega \geq 0.99$

  $\omega \geq 0.10$


316 stainless steel

FIGURE 9. Comparison of a theoretical prediction of the distribution of damage in a circular notched bar with that observed in a micrograph taken from a diametral plane close to failure.





aluminium

  $\omega \geq 0.99$


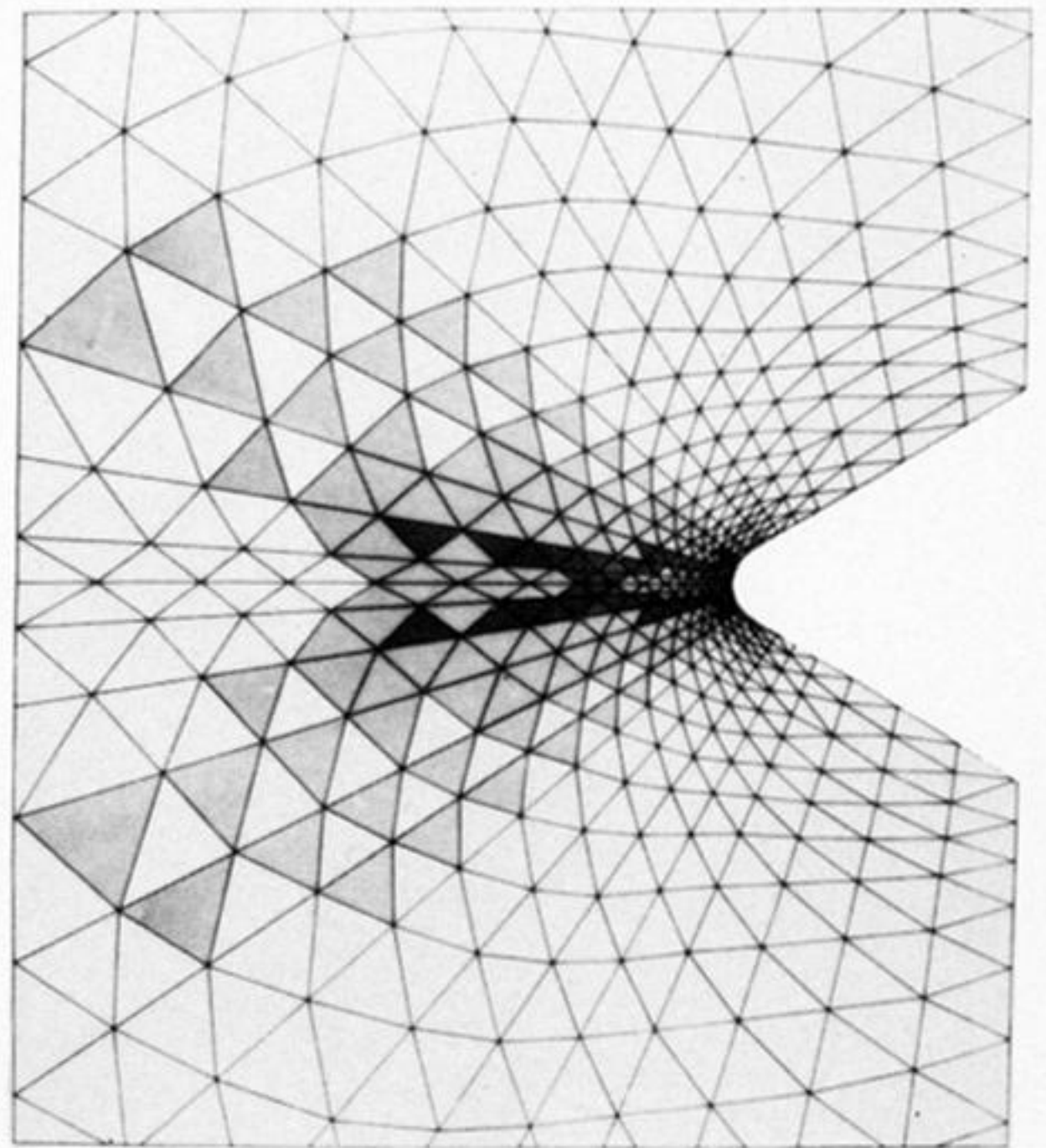
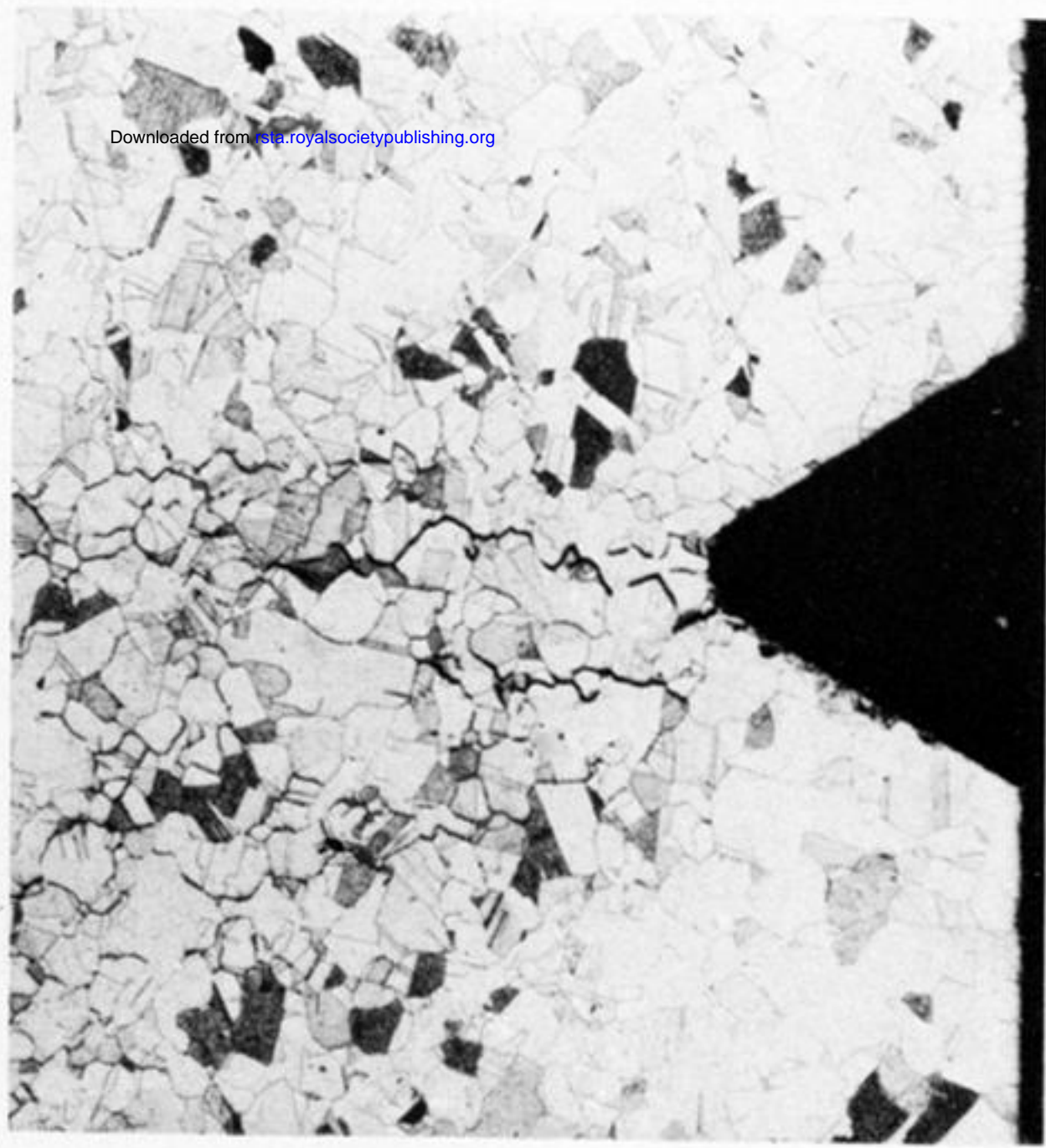

  $\omega \geq 0.10$

FIGURE 13. Comparison of a theoretical prediction of the distribution of damage in a B.S. notched bar with that observed in a micrograph taken from a diametral plane close to failure.





copper

  $\omega \geq 0.99$


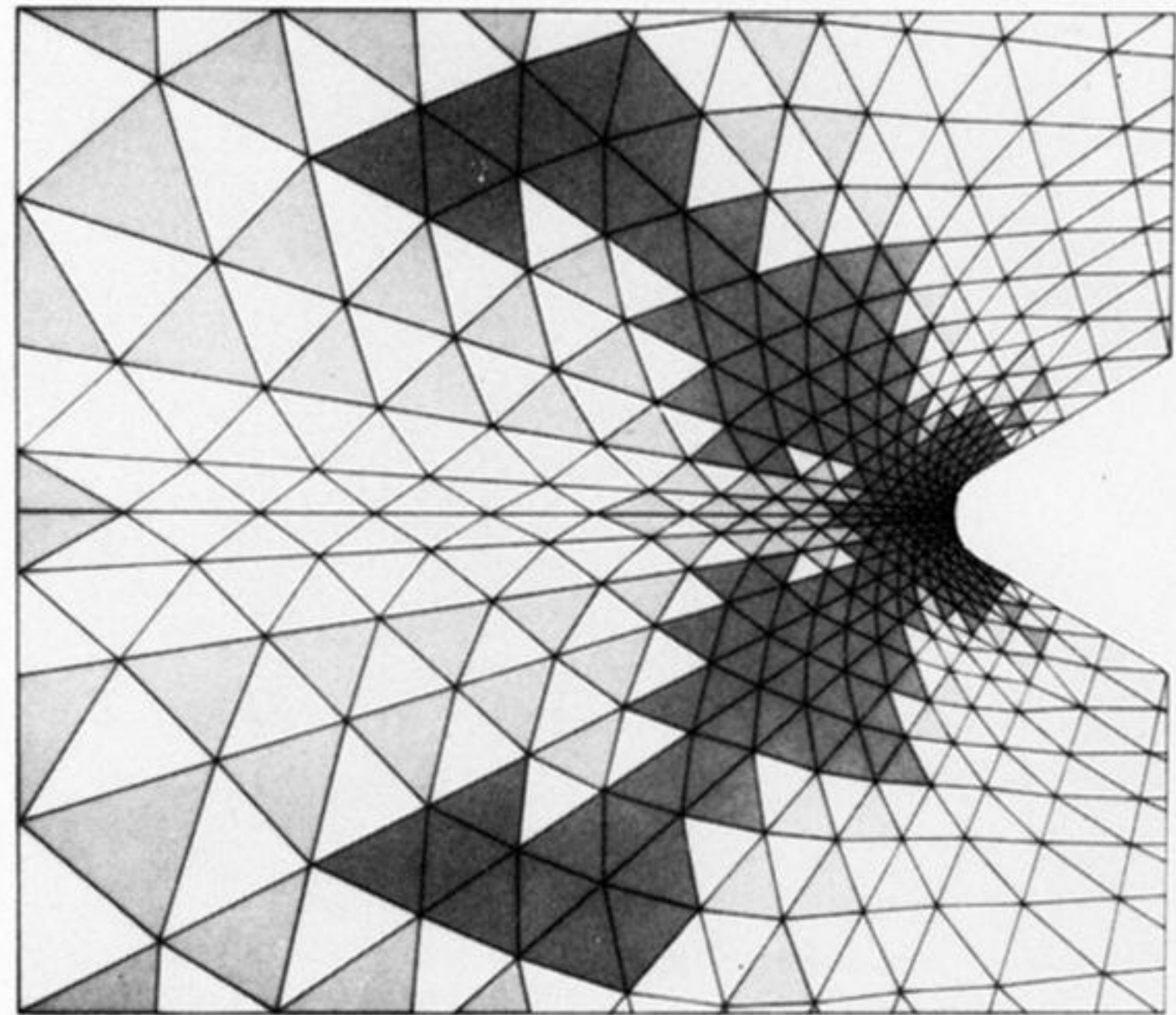

  $\omega \geq 0.10$


FIGURE 14. Comparison of a theoretical prediction of the distribution of damage in a B.S. notched bar with that observed in a micrograph taken from a diametral plane close to failure.





316 stainless steel

  $\omega \geq 0.99$

  $\omega \geq 0.10$

**FIGURE 15.** Comparison of a theoretical prediction of the distribution of damage in a B.S. notched bar with that observed in a micrograph taken from a diametral plane close to failure.